

# 1    **Redox conditions and ecological resilience during Oceanic**

## 2    **Anoxic Event 2 in the Western Interior Seaway**

3    L.J. Robinson<sup>a#</sup>, K.S. George<sup>a</sup>; C.P. Fox<sup>b</sup>, J.E.A. Marshall<sup>a</sup>; I.C. Harding<sup>a</sup>; P.R. Bown<sup>c</sup>, J.R. Lively<sup>d</sup>, S.  
4    Marroquín<sup>e</sup>, R.M. Leckie<sup>f</sup>, S. Dameron<sup>f</sup>, D.R. Gröcke<sup>g</sup>, N. M. Papadomanolaki<sup>h\*</sup>, N.A.G.M van  
5    Helmond<sup>h</sup>, and J.H. Whiteside<sup>a</sup>

6    <sup>a</sup> *School of Ocean and Earth Science, University of Southampton, National Oceanography Centre,*  
7    *Southampton, SO14 3ZH, U.K.*

8    <sup>b</sup> *Department of Earth Science, Khalifa University of Science and Technology, Abu Dhabi, U.A.E.*

9    <sup>c</sup> *Department of Earth Science, University College London, U.K.*

10    <sup>d</sup> *Prehistoric Museum, Utah State University Eastern, Price, UT, U.S.A.*

11    <sup>e</sup> *Division of Geological and Planetary Sciences, California Institute of Technology, Pasadena, CA,*  
12    *U.S.A.*

13    <sup>f</sup> *Department of Geosciences, University of Massachusetts, Amherst, U.S.A*

14    <sup>g</sup> *Department of Earth Sciences, Durham University, Durham, DH1 3LE, UK*

15    <sup>h</sup> *Department of Earth Sciences, Utrecht University, Utrecht, The Netherlands*

16    <sup>\*</sup> *Now at: Aix Marseille University, CNRS, IRD, Coll France, INRA, CEREGE, Aix en Provence, France*

17

18    *#To whom correspondence should be addressed: ejr1n17@soton.ac.uk*

### 19    **Abstract (218 words)**

20    Oceanic Anoxic Events (OAEs) are important geological events that may be analogues to future  
21    climate-driven deoxygenation of our oceans. A vast portion of the global ocean experienced anoxic  
22    conditions during the Cenomanian–Turonian OAE (OAE2; ~94 Ma), whereas the Western Interior

Seaway (WIS) experienced oxygenation at this time. Here, organic geochemical and palynological data generated from Cenomanian–Turonian age sediments from five sites in the WIS are used to investigate changing redox and ecological conditions across differing palaeoenvironments and palaeolatitudes. Heterogeneity across the sites is clear to see. However, despite this, relationships and trends among oceanographic variables are recognised: 1) Increasing total organic carbon (TOC) and CaCO<sub>3</sub> percentages indicate the onset of a sea-level maximum towards the end of OAE2; 2) C<sub>28</sub> sterane is shown to be a useful marker for prasinophyte abundance, and concurrent increases in this marker and overall sterane abundance indicate prasinophyte-driven increase in algal productivity in a stratified water column; and 3) sterane ratios can be a more reliable geochemical proxy than redox proxies for assessing the Benthic Oxidic Zone. Our redox data do not necessarily follow established trends for the WIS overall, particularly for proximal settings. We therefore surmise that local effects, such as nutrient-driven expansion of the oxygen minimum zone and/or sedimentation-driven anoxia just below the sediment-water interface, have overprinted regional trends.

## **1.1 Introduction (1,648)**

Oceanic Anoxic Events (OAEs) are acute events (<1 million years duration) associated with episodes of rapid climatic warming, widespread marine deoxygenation, perturbations of a variety of biogeochemical cycles, deposition of organic-rich sediments and biotic turnovers (Schlanger and Jenkyns, 1976; Leckie et al., 2002; Jenkyns, 2010; Robinson et al., 2017). Although OAEs predominantly occurred in the Mesozoic Era (~252 – 66 Ma), similar environmental changes are being reported in our currently rapidly changing climate (IPCC, 2021). Elevated modern global temperatures (Hawkins et al., 2017), coupled with decreasing oxygen content in the modern ocean (Keeling et al., 2010; Schmidtke et al., 2017; Breitburg et al., 2018) and indications of species loss (Barnosky et al., 2011; Dirzo et al., 2014; Ceballos et al., 2017) suggest that a better understanding of past environmental trends during OAEs can provide key insights into the trajectory of global climate in the coming decades and beyond.

49 The mid-Cretaceous Oceanic Anoxic Event 2 (OAE2; ~94 Ma) occurred during the Cenomanian–  
 50 Turonian (C–T) thermal maximum (Jenkyns, 1980; O’Brien et al., 2017), and is thought to have  
 51 been triggered by large scale volcanism that injected CO<sub>2</sub>, sulfides and trace metals into the ocean  
 52 and atmosphere (Kuroda et al., 2007; Turgeon and Creaser, 2008; Jarvis et al., 2011; Du Vivier et  
 53 al., 2014). The associated increases in temperature resulted in: (1) sluggish oceanic circulation  
 54 (Erbacher et al., 2001; Kidder and Worsley, 2010); (2) a strengthened hydrological cycle,  
 55 promoting continental run-off and nutrient addition to the oceans (Arthur et al., 1987; Adams et  
 56 al., 2010; Trabucho-Alexandre et al., 2010; Monteiro et al., 2012; van Helmond, 2013); and (3)  
 57 transgression over shallow epicontinental seas (Arthur and Sageman, 2005). Primary productivity  
 58 flourished under these conditions, culminating in widespread algal productivity, anoxic bottom  
 59 waters, higher rates of organic carbon burial and a globally recognised positive carbon isotope  
 60 excursion (CIE) (Jenkyns, 2003, 2010; Robinson et al., 2017).

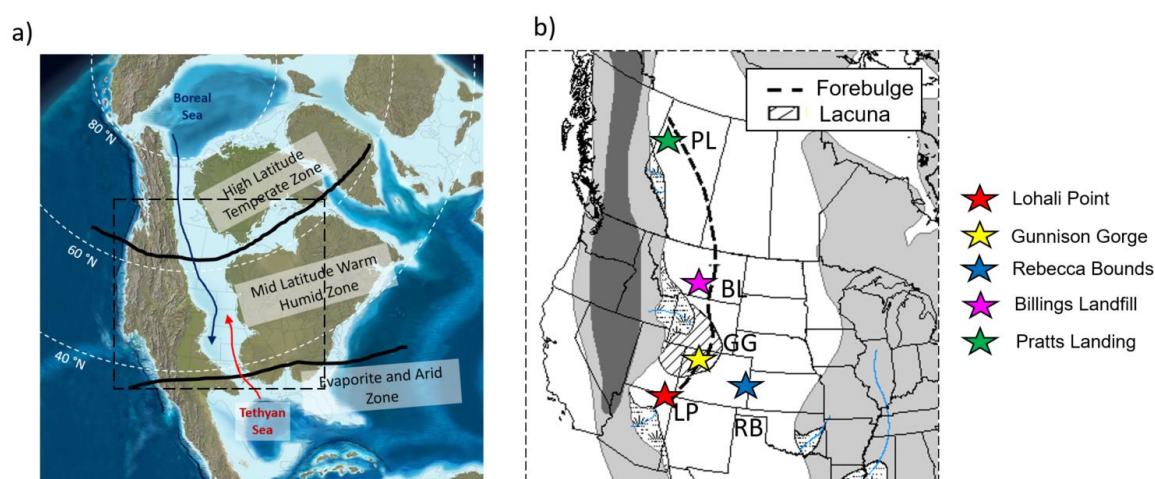
61 Organic matter produced during OAE2 is preserved globally (Schlanger et al., 1987; Takashima et  
 62 al., 2006; Robinson et al., 2017). It is estimated that 40 – 50 % of the world’s ocean by volume  
 63 could have experienced anoxic conditions (Monteiro et al., 2012; Ostrander et al., 2017), with 2–  
 64 5% of the world’s ocean becoming euxinic (Owens et al., 2013; Dickson et al., 2016a, 2016b).  
 65 However, unlike the globally synchronous CIE, deposition of organic matter varied spatially  
 66 (Vizcaíno et al., 2020), and in some cases was diachronous within basins (Tsikos et al., 2004a).

67 The Western Interior Seaway (WIS) of North America is enigmatic in that it does not conform to  
 68 global trends of deoxygenation and organic enrichment during OAE2 (Vizcaíno et al., 2020). Whilst  
 69 anoxia and deposition of organic matter was increasing across the world, the WIS experienced  
 70 intervals of oxygenation and lower organic enrichment during OAE2. Here, we present an  
 71 extensive, high-resolution organic geochemical and palynological study across a depth-transect  
 72 spanning 21° of palaeolatitude through the WIS to determine the extent of anoxia, its drivers, and  
 73 associated ecological reorganization before, during and after OAE2.

### 74 1.1.1 Geological background

75 The WIS was a shallow epicontinental seaway comprised of a rapidly subsiding clastic-rich  
 76 foredeep, discrete zones of forebulge uplift, a wider more moderately subsiding central axial  
 77 basin and a stable, broad cratonic platform to the east (Figure 1; Arthur and Sageman, 2005;  
 78 Kauffman, 1984). Marine inputs to the basin originated from both northern Boreal and southern  
 79 Tethyan ocean sources, whose relative contributions varied over time. As a relatively shallow and  
 80 restricted basin the WIS regularly experienced low oxygen conditions and organic enrichment  
 81 throughout the Cretaceous, however several studies have shown oxygenation of the water  
 82 column and a pause in organic enrichment in the central WIS during the initial onset of OAE2  
 83 (Eicher and Diner, 1985; Leckie et al., 1998; Savrda, 1998; Elderbak et al., 2014; Eldrett et al.,  
 84 2014; Lowery et al., 2017, 2018).

85



86

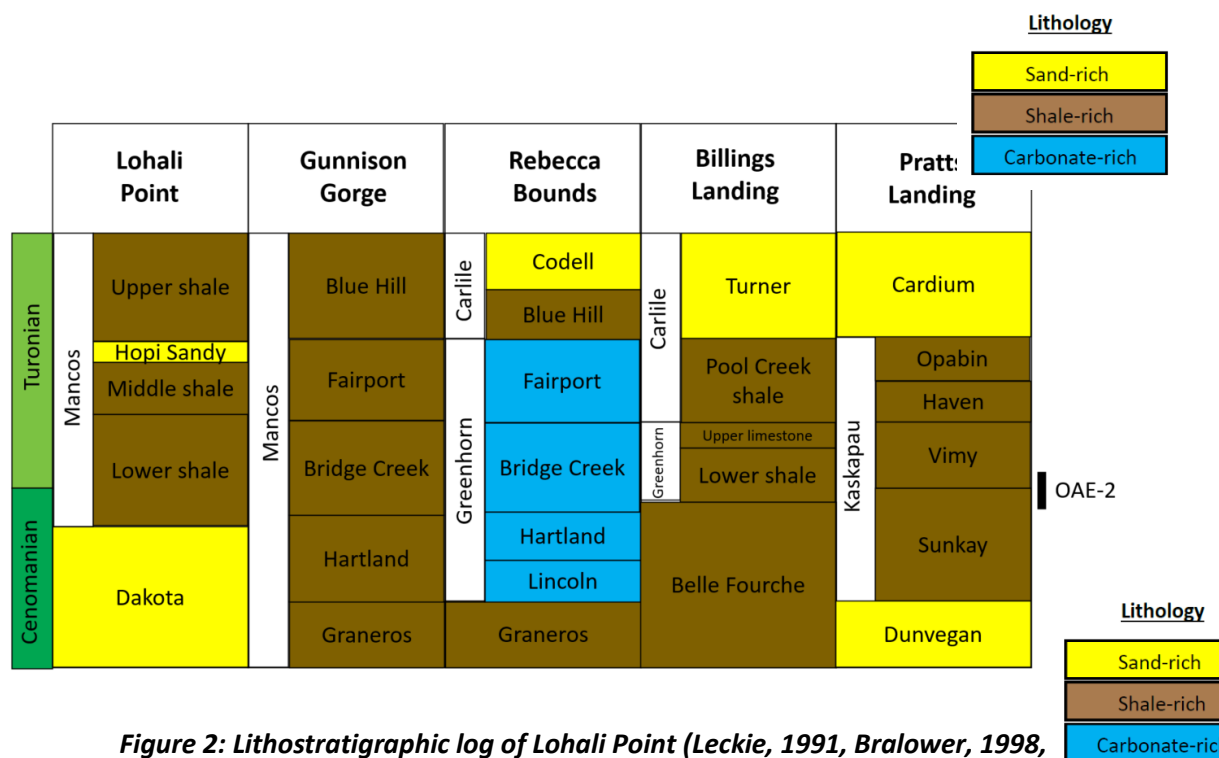
87 **Figure 1: Palaeogeography of, and study locations in, the Western Interior Seaway.**

88 **a) Palaeogeographic map depicting climate zones across the Western Interior**  
 89 **Seaway in the Cenomanian (~94 Ma to ~100 Ma), modified from Hay and Flogel**  
 90 **(2012). Red line indicates the southern-sourced Tethyan water and the blue line**  
 91 **represents the northern-sourced Boreal water. The dashed box represents the**  
 92 **location for Figure 1b. b) Location of the five study sites in the Cenomanian–**  
 93 **Turonian WIS, with proposed location of lacuna (area of non-deposition) and**  
 94 **forebulge.**

95 The expression of this oxygenation event in WIS sediments is sometimes termed the Benthonic  
 96 Zone (BOZ: Eicher and Worstell, 1970), characterised by a decrease in total organic carbon (TOC)  
 97 and redox-sensitive trace metal concentrations, concurrent with an increase in diversity and  
 98 abundance of faunal assemblages and increased bioturbation (Eicher and Worstell, 1970; Keller  
 99 and Pardo, 2004; Eldrett et al., 2014; Elderbak and Leckie, 2016). Evidence for the BOZ has been  
 100 reported from the upper Cenomanian *Sciponoceras* biozone within the US parts of the WIS (the  
 101 location of the Lohali Point, Gunnison Gorge, Rebeca Bounds and Billings Landing sites), however  
 102 evidence is absent, or rare, in the Canadian parts of the WIS, such as where the Pratts Landing site  
 103 is located (e.g. Eicher and Worstell, 1970; Eicher and Diner, 1985; Leckie et al., 1991, 1998;  
 104 Schröder-Adams et al., 1996; Elderbak et al., 2014; Elderbak and Leckie, 2016).

105

106



107

108

109

110

111

112

**Figure 2: Lithostratigraphic log of Lohali Point (Leckie, 1991, Bralower, 1998, Kirkland, 1991), Gunnison Gorge (Noe, 2015), Rebecca Bounds core (Kennedy et al., 2005), Billings Landfill (Leckie and Leithold, unpublished) and Pratts Landing (Varban and Plint, 2008).**

113 Oceanographic models for the US part of the WIS suggest the BOZ was caused by the interplay of  
114 different water masses, driven by sea-level variations. OAE2 occurred within the eustatic 3<sup>rd</sup>-order  
115 Greenhorn transgression (Figure 2; Hancock and Kauffman, 1979; Kauffman and Caldwell, 1993;  
116 Gale et al., 2008b). During the early stages of transgression the basin was relatively restricted and  
117 shallow, with low polar to tropical temperature gradients causing sluggish, stratified and low-  
118 oxygen conditions (Eicher and Diner, 1985; Kump and Slingerland, 1999; Allison and Wells, 2006).  
119 As the transgression progressed, a southern sill was breached and an influx of Tethyan waters to  
120 the east resulted in a strong Boreal-Tethyan oceanographic front in the seaway that may have  
121 extended from the central US to as far north as southern Canada (Fisher et al., 1994; Arthur and  
122 Sageman, 2005; Elderbak and Leckie, 2016; Lockshin et al., 2017; Bryant et al., 2021). The density  
123 differences between the southern saline, oxygen-poor Tethyan and northern, less-saline, oxygen-  
124 rich Boreal waters resulted in the creation of a third, denser water mass at the mixing front (a  
125 process called caballing), termed the Western Interior Intermediate Water (Hay et al., 1993). The  
126 denser water mass then sank, downwelling oxygenated surface waters, creating strong bottom-  
127 water currents, disrupting any benthic anoxia that may have been present, and resulted in the  
128 BOZ (Eicher and Worstell, 1970; Eicher and Diner, 1985; Elderbak and Leckie, 2016; Lowery et al.,  
129 2018; Bryant et al., 2021). Driven by the density differences of these water masses and freshwater  
130 influx from the hinterland, a counter-clockwise semi-estuarine circulation has been proposed to  
131 have occurred during the highest sea-levels (Slingerland et al., 1996; Floegel et al., 2005; Elderbak  
132 and Leckie, 2016; Lowery et al., 2018). Foraminiferal studies in Kansas (Elderbak et al., 2014;  
133 Lowery et al., 2018) support this model and suggest increased anoxia to the south east, and the  
134 influence of oxygen-poor Tethyan water.

135 Following the BOZ interval, dysoxic to anoxic conditions again prevailed in the US part of the WIS,  
136 as sea-level continued to rise and increased volumes of oxygen-poor Tethyan water were  
137 transported into the seaway (Lowery et al., 2018). The increased abundance of low-oxygen  
138 favouring *Planoheterohelix* foraminifera (termed the '*Heterohelix* shift' by Leckie et al. 1998) is

noted at many sites, attributed to an expanded Oxygen Minimum Zone (OMZ) influenced by low-oxygen Tethyan waters (Leckie et al., 1991) and/or increased productivity (Boudinot et al., 2020).

The Canadian part of the WIS experienced different oceanographic conditions, and was likely cooler and less saline (Schröder-Adams et al., 1996). This, coupled with the stratified and anoxic conditions indicated by geochemical redox proxies, culminated in low abundances of agglutinated benthic foraminifera and an absence of bioturbation (Schröder-Adams et al., 1996; Simons et al., 2003). As sea-level rose through the late Cenomanian to early Turonian, planktic foraminifera and nannofossils appeared at some southern Canadian sites, signalling the influence of more normal saline marine Tethyan waters (McNeil and Caldwell, 1981; Caldwell et al., 1993; Schröder-Adams et al., 1996; Dionne et al., 2016). However, abundance and diversity was low, interpreted to be due to stable stratification (perhaps enhanced by a freshwater lid), anoxic conditions and inhospitable conditions for benthic or planktic fauna to thrive (Schröder-Adams et al., 2001; Schröder-Adams, 2014; Dionne et al., 2016). The oceanographic mixing front and caballing effect are not interpreted to have reached the Canadian part of the WIS (Dameron et al., in press).

### 1.1.2 Sample sites

To facilitate an integrated study, five sites spanning different water depths, palaeoenvironments and palaeolatitudes have been selected (Table 1).

**Table 1: Key characteristics of the five sites studied here. Geographical latitude and longitude are given, with the number of significant figures representative of the known accuracy of the co-ordinates. For further details and references please see Supplemental Material A.**

Site	Present-day Location	Palaeo latitude	Water depths	Depositional environment
<b>Lohali Point (Outcrop)</b>	36.183°N, 109.883°W (NE Arizona)	~43°N	< 100 – 200 m	Neritic environment, at the distal end of a broad, shallow, seaward-sloping shelf, and inwards of the forebulge trend
<b>Gunnison Gorge (Outcrop)</b>	38.7827°N, 107.86898°W (W Colorado)	~46°N	0 – 50 m	Proximal site that was located on a large palaeo-bathymetric high, created by the rising basin forebulge

<b>Rebecca Bounds (Core)</b>	38.489628°N, 101.974552°W (W Kansas)	~45°N	< 200 – 300 m	Distal axial basin
<b>Billings Landfill (Outcrop)</b>	45.72°N, 108.56°W (S Montana)	~55°N	< 100 m	Proximal location inwards of the basin forebulge
<b>Pratts Landing (Outcrop)</b>	56.020556°N, 118.813056°W (NW Alberta)	~64°N	< 70 m	Close to the forebulge, on the eastern flank of the foredeep, approximately 160 km from the WIS shoreline

### 1.1.3 Organic geochemistry of the WIS

Lipid biomarkers provide insights into oxygenation, drivers of organic enrichment and perturbations of the carbon cycle (e.g., Eglinton and Eglinton, 2008; Peters et al., 2005). Previous studies of OAE2 within the WIS that include lipid biomarker analysis are primarily localised within the southwestern and central part of the basin (Curiale, 1994b; Pancost et al., 1998; Simons and Kenig, 2001; Sun et al., 2016; French et al., 2019; Boudinot et al., 2020; Forkner et al., 2021), or within Alberta and Saskatchewan (Simons et al., 2003; Furmann et al., 2015). Many studies support the model of increased oxygenation during the onset of OAE2, or at the Cenomanian/Turonian boundary (CTB: Simons and Kenig, 2001; Sun et al., 2016; French et al., 2019; Forkner et al., 2021). Whilst foraminiferal studies indicate Tethyan-influenced anoxia to the southeast of the WIS, lipid biomarker proxies show regional variations with heightened anoxia and photic zone euxinia in some proximal locations on the western part of the basin (e.g. Pancost et al., 1998; Boudinot et al., 2020) and Canadian sites show high levels of anoxia independent of Tethyan water influence (Simons et al., 2003). Anomalously high concentrations of C<sub>28</sub> steranes, interpreted to indicate an abundance of prasinophytes (simple unicellular green algae, often present in abundance under stressed environmental conditions, although other sources for C<sub>28</sub> steranes such as chlorophyll *c*-containing algae are recognized: Volkman et al., 1994, 1998), suggest generally inhospitable environmental conditions linked to anoxia at sites across the WIS (Curiale, 1994b; French et al., 2019; Boudinot et al., 2020; Robinson et al., in prep). There remain unresolved questions in these organic geochemical datasets, relating to the heterogeneity of



180 anoxia across the basin and the significance of high C<sub>28</sub> sterane concentrations, that this study  
181 aims to address.

182

## 183 **1.2 Methods (69)**

184 This study applies organic geochemical methods (i.e., lipid biomarker analysis) to investigate the  
185 five selected sample sites across the KWIS. This is supplemented by bulk isotopic and elemental  
186 analysis, palynology, micropaleontology, and statistical analysis. Table 2 details the key lipid  
187 biomarker and supporting palynofacies proxies used, with additional detail about these proxies  
188 contained within Supplemental Material B. A detailed description of the methods is contained  
189 with Supplemental Material C.

190

**Table 2: Geochemical and palynological proxies used in this study**

Indicator	Tech-nique	Proxy	Description	Ref.
Terrestrial input	Lipid biomarkers	<b>TAR</b> (Terrigenous Aquatic Ratio) $(nC_{27}+nC_{29}+nC_{31}) / (nC_{17}+nC_{19}+nC_{21})$	Higher TAR indicates more input from the terrigenous-derived C <sub>27</sub> , C <sub>29</sub> and C <sub>31</sub> n-alkanes.	(Peters et al., 2005)
		<b>Oleanane Index</b> ( <i>oleanane</i> / [ <i>oleanane</i> + C <sub>30</sub> αβ hopane])	Derived from angiosperms (flowering plants).	(Riva et al., 1988; Moldowan et al., 1994)
	Palynofacies	<b>C/M</b> ( <i>no. terrestrial phytoclasts + pollen + spores</i> ) / ( <i>no. of dinocysts, prasinophytes, acritarchs</i> ) *with the exception of Pratts Landing (see 1.4.3 Palynology)	% organic matter derived from terrestrial plants, compared to all terrestrial and marine organic matter	(Tyson, 1995)
Redox	Lipid biomarkers	<b>Pr/Ph</b> ( <i>pristane/phytane</i> )	Phytane is preferentially preserved in anoxic settings. Broadly: <~1 anoxic, >3 oxic	(Didyk et al., 1978; Ten Haven et al., 1987)
		<b>C<sub>34</sub>/C<sub>35</sub> HH</b> ( <i>C<sub>34</sub>αβ R/C<sub>35</sub>αβ R homohopane</i> )	C <sub>35</sub> hopane is preferentially preserved in anoxic settings. <~1 anoxic	(Peters et al., 2005)
		<b>Isorenieratane</b> ( <i>P=present; T=trace; A=Absent</i> )	Produced by anaerobic brown-pigmented green sulfur bacteria in the photic zone. Presence indicates photic zone euxinia.	(Grice et al., 1996)
Strat-ification	Lipid biomarkers	<b>Gammacerane Index</b> ( <i>gammacerane</i> / [ <i>gammacerane</i> + C <sub>30</sub> αβ hopane])	Most often attributed to ciliates at a chemocline in the water column, although the precursor for gammacerane (tetrahymanol) has other sources such as photosynthetic bacteria and freshwater ciliates.	(Sinninghe Damsté et al., 1995; Peters et al., 2005)
Ecological change	Lipid biomarkers	<b>Sterane / Hopane</b> ( <i>ratio of regular ααα steranes over regular hopanes</i> )	Ratio of molecules of eukaryotic (primarily algal / or plant) / bacterial origin	(Peters et al., 2005)
		<b>Sterane abundance relative abundance of ααα R isomers</b>	Derived from eukaryote sterols, with C <sub>27</sub> , C <sub>28</sub> , C <sub>29</sub> representing differing precursor organisms.	(Volkman, 2003)
	Paly-nofacies	<b>Prasinophyte %</b> <i>no. prasinophytes / total no. of particles counted in sample</i>	Simple unicellular green algae, often present in abundance under harsh environmental conditions	(Tappan, 1980; Tyson, 1995)

193

194

195

196 **1.3 Results and discussion (5,354)**

197 **1.3.1 Thermal maturity of studied sections**

198 Prolonged thermal stress, such as experienced during diagenesis, can rearrange the  
 199 stereochemical configurations of steranes and terpanes until a critical point whereby the  
 200 proportion of each isomer achieves a thermodynamically balanced distribution (Peters et al.,  
 201 2005). Thus it is possible to ascertain thermal maturity through certain biomarker ratios (Peters et  
 202 al., 2005; Table 3). Consistent with low thermal maturity, the 17 $\beta$ (H),21 $\beta$ -homohopane (C31 $\beta\beta$   
 203 hopane) and 17 $\beta$ (H),21 $\beta$  hopane (C30 $\beta\beta$  hopane) isomers are predominant (Mackenzie et al.,  
 204 1980; Ourisson et al., 1979; Peters and Moldowan, 1991; Seifert and Moldowan, 1980), and the  
 205 C31  $\alpha\beta$  / ( $\alpha\beta$ + $\beta\beta$ ) ratio, is relatively low <0,50. All locations studied here are thermally immature  
 206 with respect to oil generation, and therefore geochemical proxies can be assumed to be  
 207 representative of palaeoenvironmental conditions at the time of deposition.

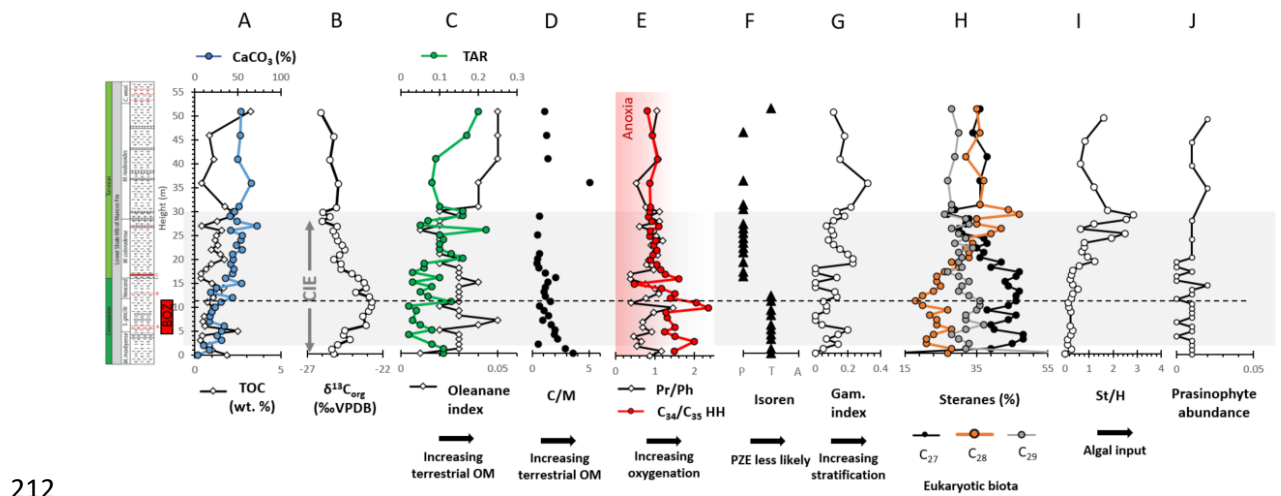
208

209 ***Table 3: Biomarker maturity parameters for five study sites***

Parameter	Approx. values for maturity	Lohali Point (n=36)	Gunnison Gorge (n=31)	Rebecca Bounds (n=44)	Billings Landfill (n=50)	Pratts Landing (n=40)
<b>Ts / (Ts + Tm)</b>	1 = late oil	0.16 $\pm$ 0.09	0.28 $\pm$ 0.09	0.31 $\pm$ 0.09	0.16 $\pm$ 0.04	0.32 $\pm$ 0.06
<b>C<sub>29</sub> Sterane 20S / (20S + 20R)</b>	0.55 = peak oil	0.06 $\pm$ 0.02	0.24 $\pm$ 0.03	0.04 $\pm$ 0.02	0.12 $\pm$ 0.03	0.11 $\pm$ 0.06
<b>C<sub>30</sub> Hopane / (Hopane + Moretane)</b>	0.95 = early oil	0.65 $\pm$ 0.06	0.77 $\pm$ 0.04	0.73 $\pm$ 0.05	0.72 $\pm$ 0.02	0.69 $\pm$ 0.1
<b>C<sub>32</sub> Hopane 22S / (22S + 22R)</b>	< 0.6 = immature	0.17 $\pm$ 0.05	0.52 $\pm$ 0.02	0.24 $\pm$ 0.1	0.39 $\pm$ 0.02	0.36 $\pm$ 0.09

## 210 1.3.2 Sample sites

### 211 1.3.2.1 Lohali Point



212

213 **Figure 3: Geochemical results for the Lohali Point site:**  
**TOC (wt. %),  $\text{CaCO}_3$  (%),  $\delta^{13}\text{C}_{\text{org}}$  (‰VPDB), TAR**  
**(terrigenous aquatic ratio:  $(n\text{C}_{27}+n\text{C}_{29}+n\text{C}_{31})/(n\text{C}_{17}+n\text{C}_{19}+n\text{C}_{21})$ ), Oleanane index (oleanane / (oleanane +  $\text{C}_{30}$   $\alpha\beta$  hopane)), C/M (continental/marine: (no. terrestrial phytoclasts + pollen + spores) / (no. of dinocysts, prasinophytes, acritarchs)), Pr/Ph (pristane/phytane),  $\text{C}_{34}/\text{C}_{35}$  HH ( $\text{C}_{34}\alpha\beta\text{R}/\text{C}_{35}\alpha\beta\text{R}$  homohopane), Isoren (presence of isorenieratane: Present, Trace, Absent), Gam. index (gammacerane / (gammacerane +  $\text{C}_{30}$   $\alpha\beta$  hopane)), Steranes (relative abundance of steranes where  $\text{C}_x = 100 \times (\text{C}_x \text{ aaaR} / (\text{C}_{27} \text{ aaaR} - \text{C}_{29} \text{ aaaR}))$ ), St/H (ratio of selected regular steranes over hopanes) and Prasinophyte abundance. For further details on the proxies used, refer to Table 1 and Supplemental Material B. Data points are not joined for C/M and Isoren as not every sample was analysed for these proxies. Ammonite zonation, Benthonic Zone (red box) and Heterohelix shift (dashed line) are taken from Leckie et al. (1991, 1998).**

224

225

226

227

228

229

230

231 At Lohali Point, a positive carbon isotope excursion (CIE) of 3.3‰ (from -26.0‰ to -22.7‰) spans

232 15 m between 5 – 20 m height (Figure 3B). Kirkland (1996) notes a disconformity at the CTB,

233 however, the shape of the Lohali Point CIE is similar to that of other sites and key features (such

234 as the peak-trough-peak-plateau shape: Pratt and Threlkeld, 1984) are also present. We thus  
 235 propose that the record is largely complete.

236 Increased foraminiferal abundance through the section suggests increasing sea-level through the  
 237 section and maximum transgression in the lower Turonian *Mammites nodosoides* to perhaps the  
 238 basal *Collignonicerias woollgari* biozone (Leckie et al., 1991; 1998). Proxies for terrestrial organic  
 239 matter (oleanane index and TAR - Figure 3C) also increase up-section which is not the usual trend  
 240 seen with transgression, when shorelines and terrestrial matter delivery systems are shifted  
 241 further away. Clay mineral, sedimentological and foraminiferal data suggest increased weathering  
 242 during this time (Leckie et al., 1991), driven by an enhanced global hydrological cycle (van  
 243 Helmond et al., 2014), and perhaps locally driven by the increase of latent heat into the seaway  
 244 from the northwards incursion of warm waters (Leckie et al., 1991), explaining the increase in  
 245 delivery of terrestrial OM up-section. There are, however, relatively low values for all terrestrial  
 246 proxies, which agrees with the assessment of Leckie et al. (1991) who found minimal presence of  
 247 plant debris in the Lower Mancos foraminiferal residues despite high sedimentation rates. This  
 248 suggests that the hinterland by Lohali Point was potentially arid and thus lacking significant  
 249 vegetation cover, which may have increased the susceptibility of the hinterland to weathering  
 250 during times of increased rainfall.

251 Values of Pr/Ph vary little (average 0.85 - Figure 3E) through the section, indicating generally  
 252 anoxic conditions. The elevated values of the C<sub>34</sub>/C<sub>35</sub> HH proxy indicate more oxygenated  
 253 conditions in the first ~ 11 m, and coincide with an increase in foraminiferal species richness and  
 254 the BOZ identified at 5 – 11 m (*Sciponoceras biozone*) (Leckie et al., 1998). Overall however this  
 255 site shows low benthic and planktic foraminiferal diversity, particularly compared to the central  
 256 part of the seaway at this time (Leckie et al., 1998; West et al., 1998).

257 Above 11 m, and mid-way through the CIE, a trend to anoxic depositional conditions corresponds  
 258 to an increase in isorenieratane derivatives, gammacerane and C<sub>28</sub> sterane abundance (Figure 3G-  
 259 I). This coincides with an increased abundance of *Planoheterohelix* foraminifera ('*Heterohelix*  
 260 shift') indicating the presence of oxygen-poor waters (Leckie et al., 1991).

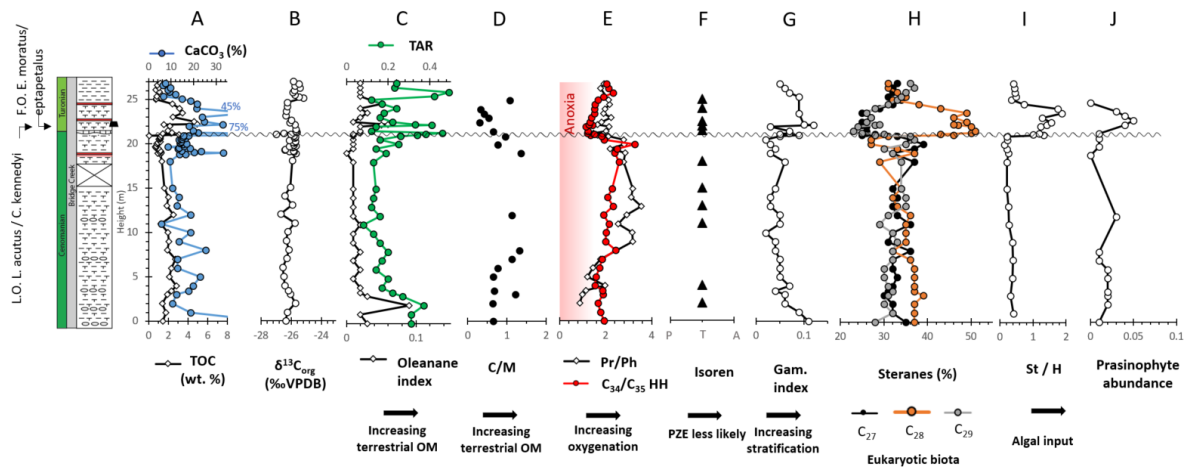


**Figure 4: Geochemical results for the Gunnison Gorge site. See Figure 3 for proxy and sedimentary log key. For further details on the proxies used, refer to Table 1 and Supplemental Material B. Last and first occurrences of selected nannofossils displayed.**

The Gunnison Gorge section has been dated using nannofossil biostratigraphy, highlighting a disconformity within a prominent ~8 cm limestone bed with an erosive base and mud rip-up clasts (see Supplemental Material A: Sample Sites). The switch from biota that have their last occurrence early in the CIE (e.g. *L. acutus* and *C. kennedyi*) to those that have their first occurrence late in the CIE (*E. moratus/eptapetalus*) suggest that at least the mid-part of the CIE (e.g., between 20.9 and 21.5 m height; Figure 4) is missing in this section. Here, a dramatic shift is seen in nearly all of the proxy data, and the  $\delta^{13}\text{C}_{\text{org}}$  CIE is not recorded (Figure 4B).

Despite a disconformity at the CIE, this site is still useful for determining the changing conditions before and after OAE2. Before the hiatus (i.e., before OAE2), sediments are generally lower in  $\text{CaCO}_3$  and TOC (Figure 4A, average 16% and 1.5% respectively), with values for both parameters decreasing to just before the disconformity. Low gammacerane values (Figure 4G) indicate a possible lack of water column stratification, and increased Pr/Ph and  $\text{C}_{34}/\text{C}_{35}$  HH (Figure 4E) suggest anoxia was not prevalent at this site and the site was in fact becoming more oxygenated

just before the disconformity. This, coupled with a slight decrease in C<sub>28</sub> sterane abundance (Figure 4H), suggest well ventilated and habitable waters just prior to the disconformity.

After the disconformity (i.e., after OAE2), a decrease in Pr/Ph and C<sub>34</sub>/C<sub>35</sub> HH values suggest less oxygenated, but not anoxic, conditions. A stark shift is seen in C<sub>28</sub> sterane abundance, however, with C<sub>28</sub> representing twice that of the C<sub>27</sub> or C<sub>29</sub> component. TOC also increases to highs of 5.2 %, but values show some variability based upon the fluctuating CaCO<sub>3</sub> component. A general increase in terrestrial proxies is seen during this interval, including variability within the TAR and the presence of wood preserved as jet. Alongside variable CaCO<sub>3</sub>, this suggests a dynamic and fluctuating palaeoenvironment driven by relative sea-level and/or pulses of fluvial input.

### 1.3.2.3 Rebecca Bounds Core

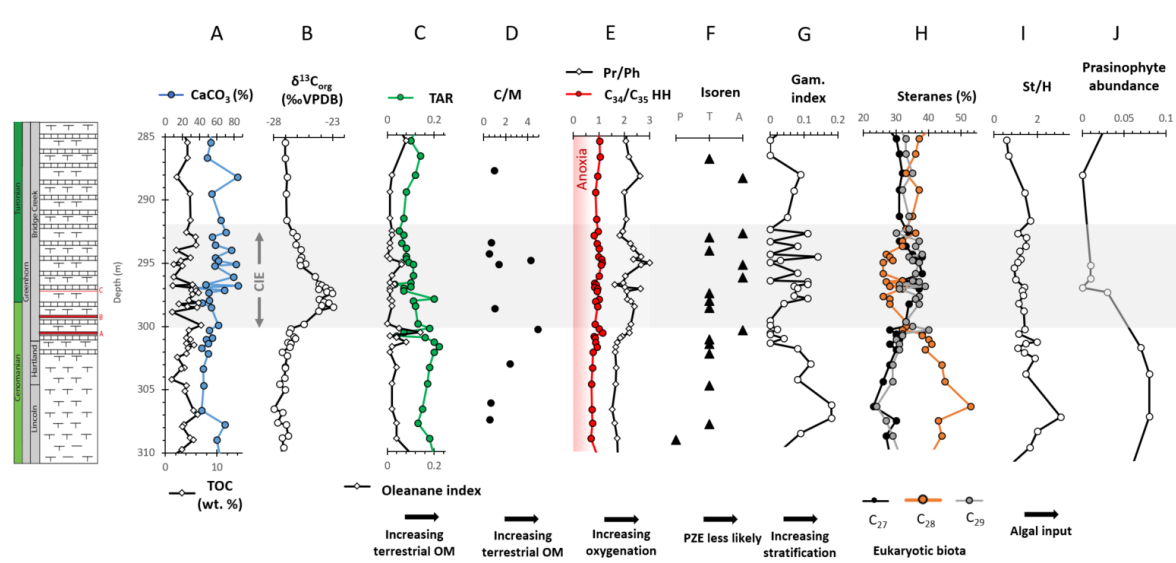


**Figure 5: Geochemical results for the Rebecca Bounds core. See Figure 3 for proxy and sedimentary log key. Major bentonites A, B and C are marked on the sedimentary log in the lower Bridge Creek Member. For further details on the proxies used, refer to Table 1 and Supplemental Material B.**

The CIE is clearly seen in the Rebecca Bounds core (Figure 5B), with  $\delta^{13}\text{C}_{\text{org}}$  values increasing by 4.3‰ from -27.3‰ to -23.0‰ (Figure 5A). The excursion follows the same trend as other  $\delta^{13}\text{C}_{\text{org}}$  isotope curves published for this location (Scott, 1998; Sageman et al., 2006; Joo and Sageman,



2014), including the presence of subpeaks that are commonly seen in CTB  $\delta^{13}\text{C}_{\text{org}}$  records across the WIS (Pratt and Threlkeld, 1984; Pratt, 1985).

CaCO<sub>3</sub> values are relatively high, with an average of 55.5%. TOC values fluctuate between 1.1% and 6.9%, with pronounced variation during the CIE (Figure 5A). Terrestrial proxies TAR, Oleanane index and C/M (Figure 5C) suggest fluctuating terrestrial organic matter input with a decrease in the later part of the CIE up to the middle part of the Bridge Creek Limestone Member.

Pr/Ph values suggest that this site was not particularly anoxic, and although there are particularly low C<sub>34</sub>/C<sub>35</sub> HH values (Figure 5E) these are likely due to high amounts of C<sub>35</sub> homohopanes associated with carbonate lithologies (Peters et al., 2005). All redox proxies (Pr/Ph, C<sub>34</sub>/C<sub>35</sub> HH, isorenieratane – Figure 5E-F) indicate increased oxygenation at the start of the CIE, continuing until the middle part of the Bridge Creek Limestone, where proxies indicate a slight decrease in oxygenation up-core. Gammacerane values are low, but suggest possible stratification before the CIE, with stratification less likely from the CIE up to the top of the section (Figure 5G). A switch from C<sub>28</sub> being the major to the minor component of the steranes occurs at the base of the CIE, however, C<sub>28</sub> then becomes dominant again at the end of the CIE (Figure 5H).

#### 1.3.2.4 Billings Landfill

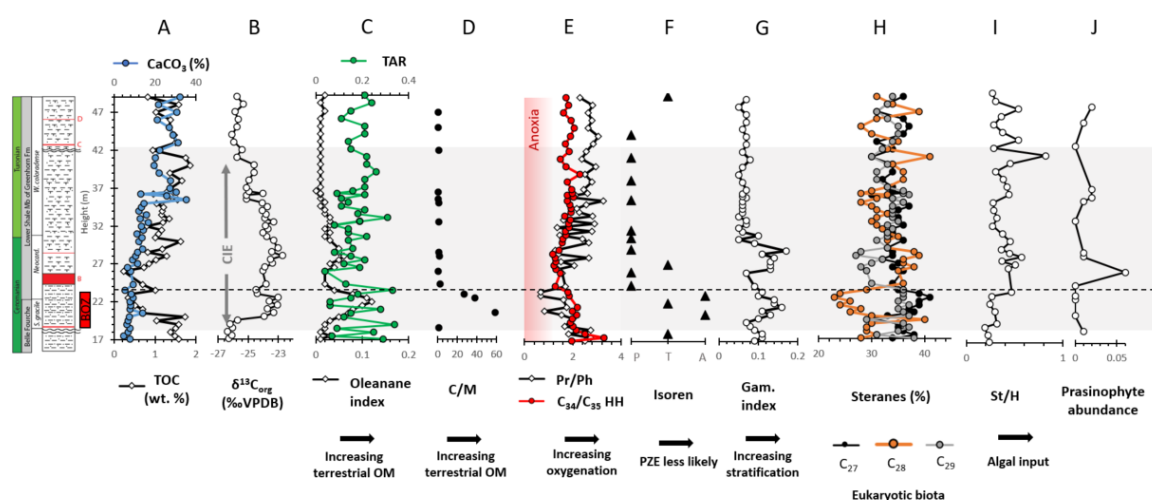


**Figure 6: Geochemical results for the Billings Landfill site. See Figure 3 for proxy and sedimentary log key. For further details on the proxies used, refer to Table 1 and Supplemental Material B. Major bentonites A, B, C and D are marked on the**

***sedimentary log in the lower shale member of the Greenhorn Formation. Ammonite zonation, Benthonic Zone (red box) and Heterohelix shift (dashed line) are taken from Dameron et al., in press.***

The CIE at Billings Landfill is identified as a ~ 3‰ positive excursion in  $\delta^{13}\text{C}_{\text{org}}$  values from the *Sciponoceras* ammonite biozone and extending to the *Watinoceras* ammonite biozone (Figure 6B). Erosive surfaces are seen at outcrop immediately prior to the CIE and a comparison of the shape of the excursion with other isotopic expressions of OAE2 from the WIS show a condensed, or truncated, onset of the CIE (Dameron et al., in press).

$\text{CaCO}_3$  is relatively low from the base of the section, rising from ~5 to ~15%  $\text{CaCO}_3$  in the lower 35 m (Figure 6A). After 35 m  $\text{CaCO}_3$  increases to an average of 26%, concurrent with a dominance in *Neobulimina* calcareous benthic foraminifera (Dameron et al., in press). TOC is also relatively low, dropping from ~1.5% to lows of 0.2% in the lower part of the CIE before rising again to values ~1.5% in the upper part of the CIE and above (Figure 6A). The initial decrease in TOC values coincides with the BOZ identified by foraminiferal workers (Dameron et al., in press). Oleanane and C/M values suggest a significant input of terrestrial organic matter at this time (Figure 6C-D), which may indicate increased run-off and clastic dilution of organic matter, contributing to the low TOC values.

Pr/Ph and  $\text{C}_{34}/\text{C}_{35}$  HH suggest an overall oxic to dysoxic site (Figure 6E). Both ratios show a decrease in oxygenation to possible anoxic to dysoxic conditions between 21 – 30 m height during the lowermost part of the CIE, corresponding with an increase in terrestrial organic matter and gammacerane. A discrete interval of greater foraminiferal abundance and diversity represents a BOZ in the lower part of the section (19.5 – 20.5 m: Dameron et al., in press), which, although brief, does coincide with a stark decrease in  $\text{C}_{28}$  sterane abundance for ~ 4 m, and absence of photic zone euxinia indicator isorenieratane (figures 6F and H).

### 1.3.2.5 Pratt's Landing

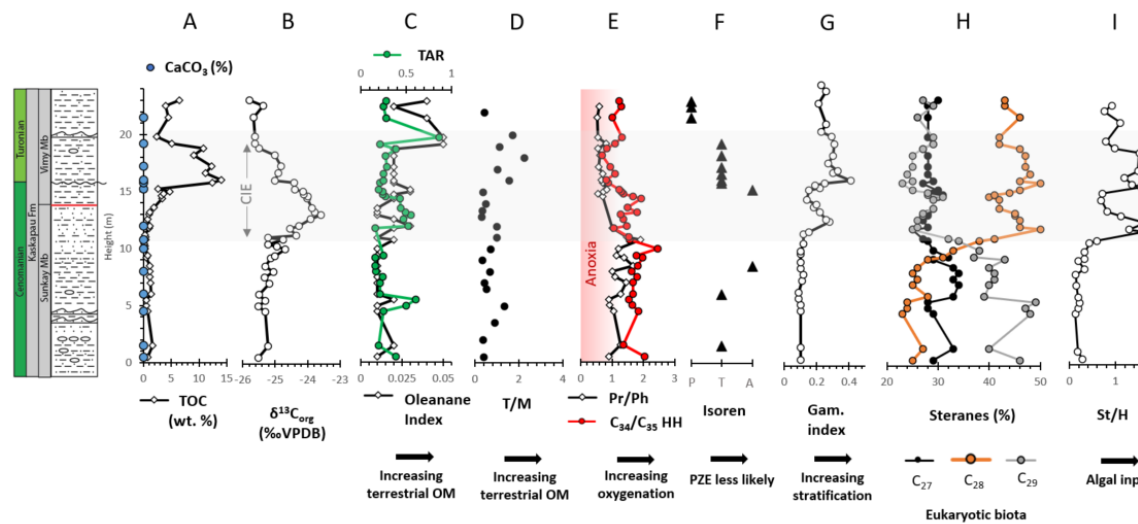


**Figure 7: Geochemical results for the Pratt's Landing site. See Figure 3 for proxy and sedimentary log key. For further details on the proxies used, refer to Table 1 and Supplemental Material B. Prasinophyte data were not collected for this section.**

At Pratt's Landing, a disconformity during the lowermost Turonian has been inferred from wireline correlation (van Helmond et al., 2016). This disconformity is represented in the CIE at the CTB by a sharp drop in  $\delta^{13}\text{C}_{\text{org}}$  values in what would have been the plateau of the CIE (Figure 7B). The start of the CIE is located within the sandstones in the upper part of the Sunkay Member and has an overall positive shift of 2 ‰.

$\text{CaCO}_3$  values for samples throughout this site are below detection limit. TOC values are low through the silty and sandy Sunkay Member (0 – 14 m, average 0.8 %), rising to 4.8 % in the claystone of the lower part of the Vimy Member (14 – 15 m: Figure 7A). A sharp and significant increase is seen in TOC values, from 2.6 to 14 %, above the hiatus in the Vimy Member at approximately 15 m.

Terrestrial proxies (oleanane, TAR and C/M – Figure 7C-D) show discrete increases in terrestrial organic matter corresponding to particularly low TOC values between 5 – 5.5 m and 19 – 22 m height, within the wave-rippled fine-grained sandstones of the Sunkay Member and the Vimy member respectively. The oleanane index is low throughout the section, despite relatively high TAR values and coarse-grained facies indicating close proximity to shore. Although angiosperms

367 had radiated to Arctic latitudes by the mid-Cenomanian (Upchurch and Wolfe, 1993), these  
368 oleanane values suggest they were unlikely to be in abundance in the hinterland close to Pratts  
369 Landing.

370 Some Pr/Ph values were not recorded in this section due to loss of shorter chain *n*-alkanes,  
371 identified by the chromatogram profile which would have resulted in depressed and non-  
372 representative Pr/Ph values. This occurs most often in the upper part of the Sunkay Member and  
373 may be related to the low organic content in these sandstones. The Pr/Ph trend for non-degraded  
374 samples, however, does match with that of the C<sub>34</sub>/C<sub>35</sub> HH, taken from larger-chain terpanes,  
375 indicating that values here are likely representative of redox conditions (Figure 7E).

376 Low gammacerane and C<sub>28</sub> steranes values below the CIE in the Sunkay Member, coupled with  
377 elevated values for redox proxies (Pr/Ph and C<sub>34</sub>/C<sub>35</sub> HH) and elevated C<sub>29</sub> steranes, indicate an  
378 oxygenated, mixed water column with the largest eukaryotic component deriving from land  
379 plants (Figure E,G,H). At the onset of the CIE however oxygenation decreases, stratification  
380 increases and C<sub>28</sub> sterane values dramatically rise from 26 to 50 % abundance through the lower  
381 part of the Vimy Member to the disconformity. Above the disconformity redox proxies are at their  
382 lowest (Pr/Ph averaging 0.63; C<sub>34</sub>/C<sub>35</sub> HH averaging 1). Above ~ 19 m height, a slight increase in  
383 C<sub>34</sub>/C<sub>35</sub> HH coincides with a lack of isorenieratane derivatives and decrease in TOC from 10.8 to  
384 2.4 %, alongside an increase in terrestrial organic matter and presence of wave-rippled, fine-  
385 grained sandstones. Isorenieratane derivatives are only present in trace amounts, or are  
386 occasionally absent, indicating prolonged PZE was unlikely at this location (Figure 7F).

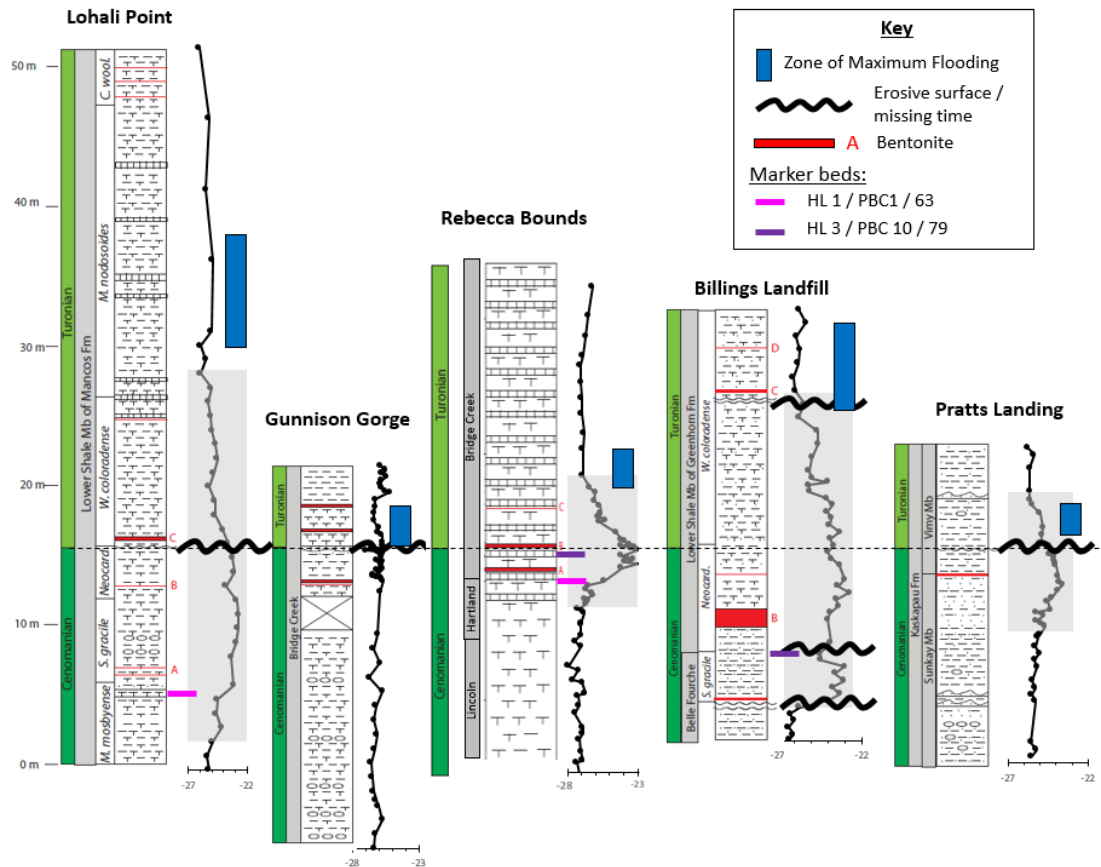


**Figure 8: Sedimentary logs and  $\delta^3C_{org}$  isotope curve for the five study sites.**

**Sedimentary log key is found in Figure 3. Grey box indicates the CIE of OAE2.**

**Marker beds use the nomenclature of Hattin (1985), Elder & Kirkland (1985) and Cobban and Scott (1972).**

The five sites here can be correlated from the positive CIEs, volcanic ash layers (i.e. bentonites), published ammonite biozones, nannofossils and/or prominent carbonate beds (Elder, 1987; Bralower and Bergen, 1998; Elderbak and Leckie, 2016). TOC and  $CaCO_3$  increase up section to maximum values above the CIE at all sites. This is interpreted to reflect a decrease in clastic input and increasing sea-level, and thus allowing a tentative positioning of the zone of maximum flooding (White and Arthur, 2006; Figure 8).

Indications of missing time such as erosive surfaces and truncated carbon isotope curves are apparent for all proximal sites (i.e., Lohali Point, Gunnison Gorge, Billings Landfill, Pratts Landing; Figure 8). Disconformities are found in the upper Cenomanian and CTB interval across the WIS,

403 attributed to winnowing (caused by either sea-level fall or rise) and/or condensation due to  
404 sediment starvation during subsequent transgression (Sageman, 1996; Schröder-Adams et al.,  
405 1996, 2012; Varban and Plint, 2008a; Eldrett et al., 2017). Oceanographic modelling suggests a  
406 strong, southward-flowing coastal jet impinged on the sea-floor in the location of the NW  
407 Colorado High (Slingerland et al., 1996) which may explain the significant disconformity at the  
408 Gunnison Gorge location, leading to the loss of sediments deposited during OAE2. No evidence of  
409 missing strata/time is evident in the Greenhorn Formation in the more distal Rebecca Bounds  
410 core (Scott, 1998).

#### 411 **1.3.4 Terrigenous input**

412 Terrestrial proxies in this study do not tend to correlate well with each other, a trend seen in  
413 other biomarker studies (Boudinot et al., 2020), and is likely due to differences in the source and  
414 transport mechanisms for terrigenous organic matter. Across its broad latitudinal extent, the WIS  
415 would have had multiple fluvial systems discharging into the basin, predominantly from the  
416 western coast where fluvio-deltaic systems transported clay-rich sediment and terrestrial organic  
417 matter from the rising Sevier mountains (e.g. Bhattacharya and Tye, 2004; Hay and Plint, 2020; Li  
418 et al., 2015; Plint, 2000), but also from the east (Elderbak et al., 2014).

419 Dominance of terrestrial over marine organic matter in a basin can be influenced by: (a) distance  
420 from the shoreline (moderated by relative sea-level); (b) transport pathways (e.g., hydrological  
421 cycle and wind); and (c) plant biomass on the hinterland. Low terrestrial proxy values generally  
422 correlate with high sea-level for the Gunnison Gorge, Rebecca Bounds and Pratts Landing sites,  
423 indicating relative sea-level (and therefore distance from shoreline) was driving terrestrial organic  
424 matter content. The opposite is apparent for Lohali Point, where increased hydrological cycling  
425 during rising sea-levels (Leckie et al., 1998; van Helmond et al., 2014) drove an increased  
426 contribution of terrestrial organic matter and overprinted any signal from sea-level variations.

### 427    **1.3.5        C<sub>28</sub> sterane abundance, prasinophytes and algal productivity**

428    C<sub>27</sub> and C<sub>29</sub> steranes correlate with each other at each section and, with the exception of Lohali  
429    Point (Figure 3H) and the pre-CIE section of Pratts Landing (Figure 7H), show similar values. C<sub>28</sub>  
430    sterane, however, covaries with both C<sub>27</sub> and C<sub>29</sub> suggesting that variations in C<sub>28</sub> sterane drive the  
431    sterane signal (figures 3 – 7), similar to findings at other WIS sites (Supplemental Material F).

432    PCA was undertaken to elucidate primary controls on the drivers of proxy variation and organic  
433    matter composition, and highlight relationships between the sterane and prasinophyte proxies  
434    (Figure 9). In all PCA plots the arrow vector for C<sub>28</sub> sterane is approximately 180° to that of C<sub>27</sub> and  
435    C<sub>29</sub> sterane, further supporting the covariation between C<sub>28</sub> sterane and C<sub>27</sub> and C<sub>29</sub> steranes by  
436    demonstrating that C<sub>28</sub> sterane controls the variability in the data in opposing ways to C<sub>27</sub> and C<sub>29</sub>  
437    steranes.

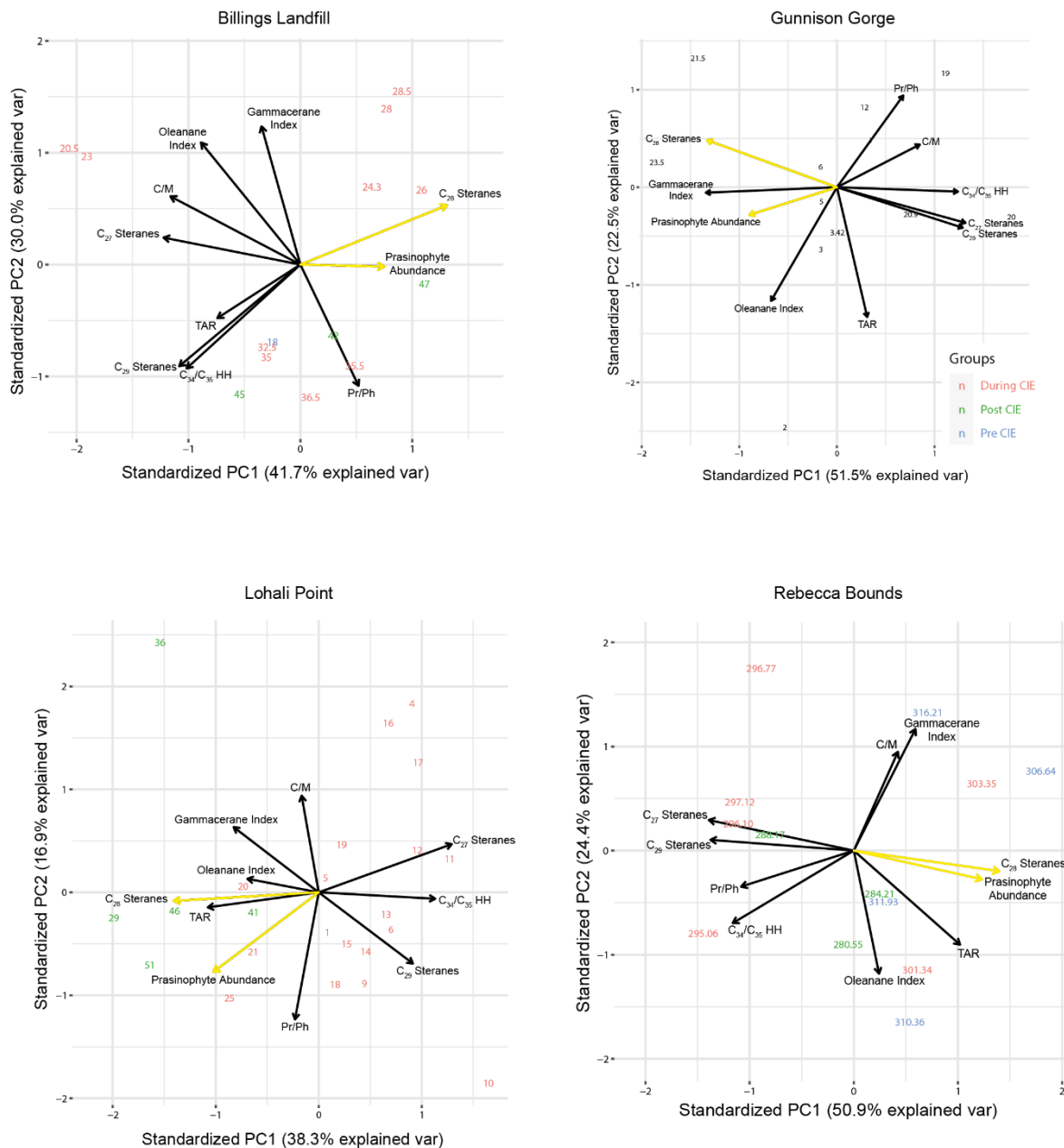


**Figure 9: Principal Components (PC) 1 and 2 for Billings Landfill, Gunnison Gorge, Lohali Point and Rebecca Bounds. Numbers represent specific depths/heights. Prasinophyte abundance and C<sub>28</sub> sterane axes highlighted in yellow. Note that in each plot these axes plot close to each other, and typically contribute the most to PC1 (highest explained variance).**

Steroids are important components within all eukaryotic cell membranes, and their wide distribution in biological systems limits the capacity to use their diagenetic products, the sterenes, steranes and diasteranes, as biomarkers for specific organisms (Volkman, 1986). Definite phylogenetic relationships can be established, however, with C<sub>27</sub> steranes (cholestane) generally indicative of red-algae, C<sub>28</sub> steranes (ergostane) of marine prasinophyte- and chlorophyll-c phytoplankton and C<sub>29</sub> steranes (stigmastane) from freshwater or other marine green algae, and land plant material (Huang and Meinschein, 1979; Tissot and Welte, 1984; Volkman, 1986;



451 Schwark and Empt, 2006; Knoll et al., 2007; Kodner et al., 2008). The relative compositions of  
 452 these molecules have varied over deep time, recording major shifts in eukaryote ecology and  
 453 evolution (Brocks et al., 2017).

454 C<sub>28</sub> steranes may derive from numerous chlorophyll *a+c* phytoplankton, such as Bacillariophyceae,  
 455 Dinoflagellata, and Haptophyta (Falkowski et al., 2004; Volkman et al., 1998). Abundance of C<sub>28</sub>  
 456 steranes has been particularly linked to prasinophyte abundance however, and are the dominant  
 457 sterane within living prasinophyte species that have been studied (Volkman et al., 1994; Schwark  
 458 and Empt, 2006). Prasinophytes are unicellular green algae (Figure 10) that have been considered  
 459 'disaster species' by Tappan (1980) due to their abundance in sediments deposited in low-oxygen  
 460 conditions associated with environmental perturbations and biotic turnovers (e.g. van de  
 461 Schootbrugge et al., 2005; Baranyi et al., 2016). Indeed, within this study high C<sub>28</sub> sterane values  
 462 correspond with less oxygenated conditions (Figure 11), although the correlation is not of high  
 463 statistical significance for most sites.

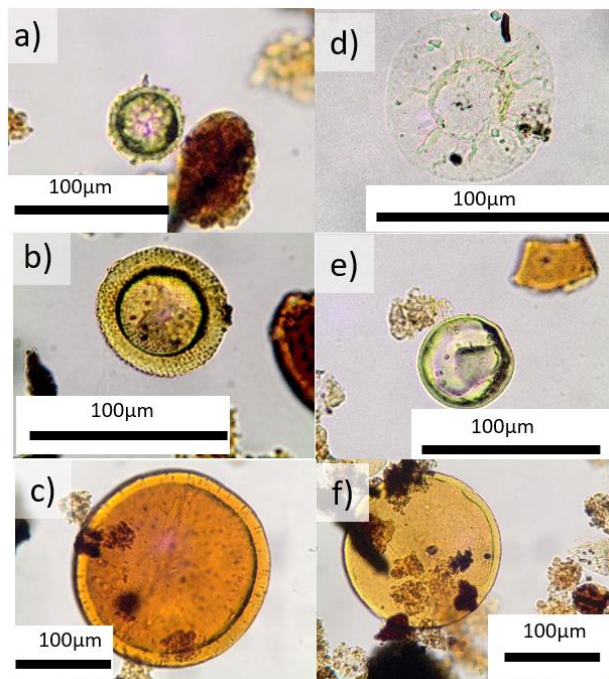


**Figure 10: Prasinophytes identified within this study; a) Herkomorph (?Cymatiosphaera); b) Tasmanitid (Lophosphaeridium); c) Tasmanitid (Crassosphaera); d) Pteromorph; e-f) Leiosphere.**

474

475 As displayed by the vector arrows protracting in near identical directions in the PCA results, C<sub>28</sub>  
 476 sterane and prasinophyte abundance proxies control variability in the data in very similar ways  
 477 suggesting a relationship between the two proxies. In addition, in each plot the C<sub>28</sub> sterane and  
 478 prasinophyte abundance arrow vectors contribute to the Principal Component (PC)-1. This  
 479 supports the positive relationship between the abundance of C<sub>28</sub> steranes and prasinophytes at  
 480 the Lohali Point, Gunnison Gorge, Billings Landfill and Rebecca Bounds sites (figures 3 – 6).

Increased prasinophyte abundances identified from palynofacies analysis correlate with high  $C_{28}$  sterane values, although high  $C_{28}$  steranes can occur in samples with low prasinophytes (such as the lower part of the Gunnison Gorge section). This may indicate additional sources of  $C_{28}$  steranes from Chlorophyll-c producing organisms, such as red/brown algae and dinoflagellates (Dougherty et al., 1970), or the presence of nano- or pico- sized prasinophytes (<2  $\mu\text{m}$ ) too small to be retained by the 15  $\mu\text{m}$  sieve used in palynological processing. The overall low abundance of prasinophytes identified within these samples must be acknowledged and may be due to said loss of nano- or pico- sized prasinophytes.

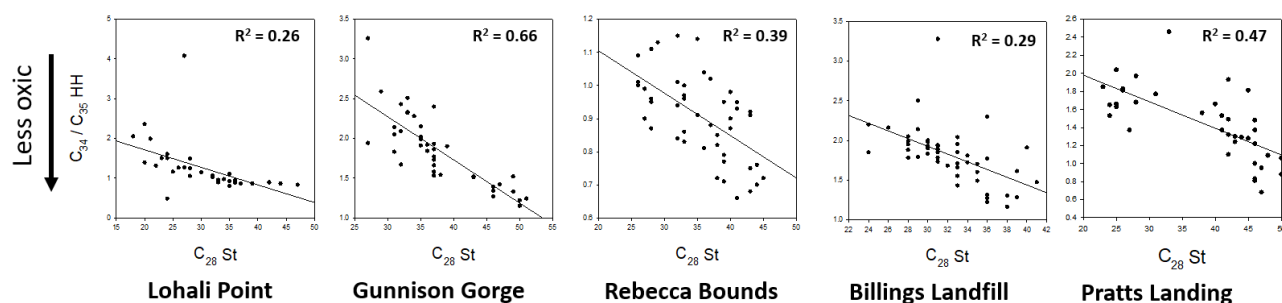


**Figure 11: Cross plots of  $C_{34}/C_{35}$  HH (redox) against  $C_{28}$  sterane (possible prasinophyte abundance) for all five sites in this study**

Comparing trends in our sterane data with the foraminiferal work conducted on Lohali Point (Leckie et al., 1998; West et al., 1998), shows that sterane trends reflect faunal variations. At Lohali Point, maxima in % planktic foraminifera at 3, 7 and 11 m correspond to maxima in  $C_{27}$  steranes and a minima in  $C_{28}$  sterane values. Furthermore, the *Heterohelix* shift at 11 m (base *Neocard.* biozone), indicative of an increase in low oxygen dwelling *Planoheterohelix globulosa*, marks a possible decrease in redox proxies, and coincides with the start of a steady increase in  $C_{28}$  sterane values.

$C_{28}$  sterane trends show a strong coupling to the ratio of eukaryotic steranes to bacterial hopanes (St/H: figures 3 – 7) – indicating heightened algal presence due to prasinophyte abundance. Increased algal abundance is typically caused by high nutrient input and Forkner et al. (2021) and Zeng et al. (2018) postulate that episodic volcanism and associated nutrient influx drove

504 variations in primary productivity during OAE2, as evidenced by an increase in C<sub>28</sub> sterane above  
 505 some bentonites. An anomalously high C<sub>28</sub> value of 40% at above a bentonite at 19.4 m at Billings  
 506 and elevated values up to 39% after Bentonite B (Figure 6H) is demonstrated, with the latter  
 507 coinciding with a significant increase in prasinophytes identified through palynology (Figure 6J).  
 508 There are also slight fluctuations in the steranes at Rebecca Bounds where C<sub>28</sub> becomes the  
 509 dominant sterane in an otherwise low C<sub>28</sub> sterane trend (between depths of 297.32 m and 296.68  
 510 m) immediately after Bentonite B (Figure 5H). These occurrences do not coincide with elevated  
 511 St/H values, however, suggesting that whilst the overall eukaryotic community may become more  
 512 dominated by prasinophytes, volcanic activity does not appear to drive increased algal  
 513 productivity. In this study redox proxies do not vary significantly above bentonites, and so  
 514 biogeochemical effects other than productivity-driven expansion of the OMZ (Zeng et al., 2018)  
 515 must also be considered to account for the increase in prasinophytes, such as volcanic-driven  
 516 water-column toxicity (e.g. Cronin et al., 2003), a change in pH (Wang et al., 2020), decreased  
 517 irradiance and/or other climate/environment shifts.

518 The strong correlation seen between C<sub>28</sub> sterane and gammacerane in this study indicates that  
 519 stratification may be a major driver of algal activity in the WIS. Gammacerane is derived from  
 520 tertrahymanol, which is primarily biosynthesised by bacterivorous ciliates in the absence of  
 521 steroid-rich algae at the interface between oxic and anoxic zones in stratified water columns (Li,  
 522 1989; Ten Haven et al., 1989; Sinninghe Damsté et al., 1995). Thus, gammacerane has often been  
 523 used as a proxy from stratification, although care must be taken in interpretation due to the  
 524 discovery of additional bacterial sources for gammacerane in sediments (Banta et al., 2015).

525 Prolonged density stratification may be associated with a dominance of prasinophytes, when  
 526 low-oxygen waters and increased amounts of reduced or regenerated nitrogen reach the lower  
 527 photic-zone (Prauss, 2007). Prasinophytes are known to become abundant under decreased  
 528 nitrate and increased ammonium availability (e.g., Cochlan and Harrison, 1991), indicating they  
 529 were better adapted to the reduced recycling of nutrients that occurs during water column  
 530 stratification (Prauss, 2007). Prolonged stratification generally favours organisms with a smaller

531 surface area to volume ratio in order to facilitate nutrient uptake, such as nano- or picoplankton  
532 (organisms < 2 µm; Wells et al., 2015), in which prasinophytes have been shown to be an  
533 important component of nano- and pico-plankton in the modern ocean (Litchman et al., 2006).  
534 Boudinot et al. (2020) suggest that prasinophyte abundance in the WIS may be affected by an  
535 increase in ammonium N-sources globally during OAE2 (Higgins et al., 2012; Naafs et al., 2019).  
536 Whilst this may play an important part in prasinophyte dynamics, data from the Rebecca Bounds  
537 core and other WIS studies (Eldrett et al., 2017; Supplemental Material F) show C<sub>28</sub> steranes and  
538 prasinophyte abundance to be higher prior to OAE2 and therefore not affected by any specific  
539 OAE2 driven increases in ammonium. We suggest that in the WIS stratification drove reduced  
540 nutrient recycling, reduced nitrate availability and, therefore, increased prasinophyte abundance.

#### 541 **1.3.6 Stratification and anoxia**

542 The proxy for stratification, gammacerane, has relatively high values (up to 0.41; Figures 12-13)  
543 when compared to biotic crises documented from more open ocean settings, such as the end-  
544 Triassic mass extinction (~0 – 0.03: Kasprak et al., 2015), and Toarcian OAE (0.01 – 0.04, French et  
545 al., 2014). Values are more in line with those found during the CTB at other WIS sites, such as  
546 west-central Alberta (0.07 – 0.21: Furman et al., 2015) and central Texas (up to 0.58: French et al.,  
547 2019), alongside those values for lacustrine deposits (0.04 – 0.42 (Chen and Summons, 2001;  
548 Huang et al., 2020; Rizzi et al., 2020; Yin et al., 2020). This suggests that the WIS experienced  
549 particularly stratified conditions during the CTB, although local variation exists (e.g., values less  
550 than 0.03 in Utah; Boudinot et al., 2020).

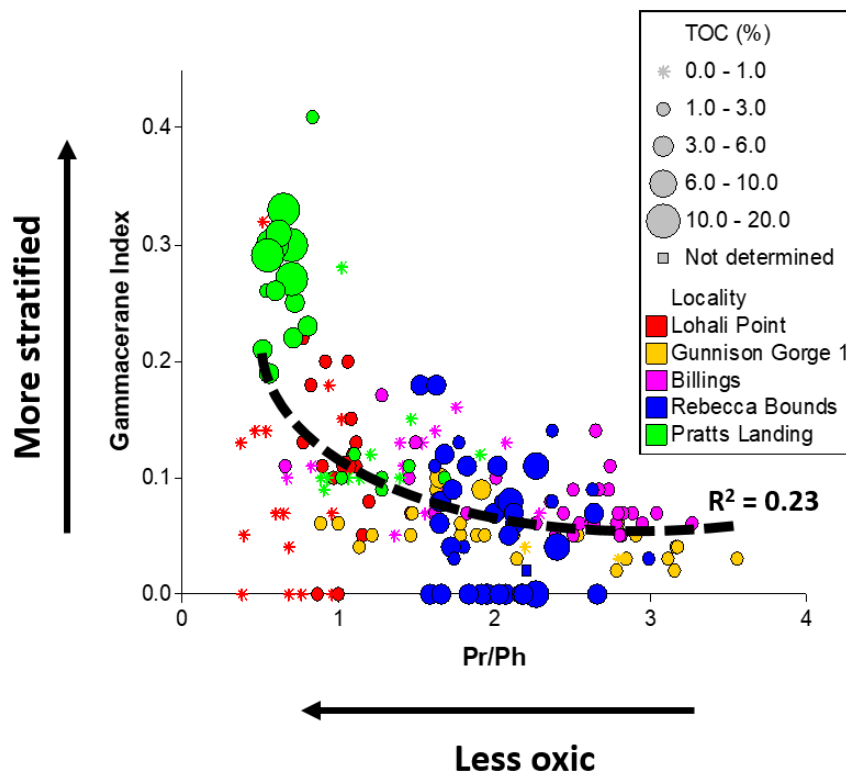


**Figure 12: Crossplot of Gammacerane Index (stratification) and Pr/Ph (redox) for all 5 sites.**

In this study stratification generally increases with sea-level (figures 3, 4, 7), as increased water depths allowed for a more stable chemocline to develop. The exception to this is at the Rebecca Bounds core, where variability during OAE2 makes trends hard to distinguish, and at Billings Landfill where stratification breaks down during highest sea-levels. The Boreal/Tethyan mixing front is hypothesized to be located close to Billings Landfill during OAE2 (Dameron et al., in press) and the effect of associated caballing during high sea-levels at this location may explain the marked decrease in stratification as sea-levels rose.

At all sites, a positive relationship is seen between the stratification proxy, gammacerane, and terrestrial input, particularly at Billings Landfill (Figure 6) where peaks in oleanane (terrestrial input) correspond closely to peaks in gammacerane. These increases in terrestrial organic matter suggest increased fluvial input, and, whilst increased water-depth is likely to be the main driver of stratification, freshwater-driven salinity stratification may also be an important factor.

566 In this study, strong stratification is linked to increased anoxia; however, anoxia can also be  
567 present in the absence of stratification, particularly in the Lohali Point site (figures 3, 12). This is  
568 perhaps due to a productivity-driven OMZ rather than a stratified water column (Leckie et al.,  
569 1991; Boudinot et al., 2020; Forkner et al., 2021), or due to proxies recording anoxic conditions in  
570 the sediments, rather than the overlying water column which was relatively well-mixed and  
571 oxygenated (Piper and Calvert, 2009; Plint et al., 2012).

572 Particularly high sedimentation rates can rapidly bury organic matter on the sea-floor, isolating it  
573 from potentially oxidizing bottom waters and causing pore-waters, only a few millimeters below  
574 the sea-floor in some instances to become anoxic (Piper and Calvert, 2009; Plint et al., 2012). This  
575 model may explain the discrepancies between high benthic faunal abundances and geochemical  
576 proxies suggesting anoxia, or at least low oxygen conditions. The BOZ at Billings, represents such a  
577 phase, where high sedimentation rates (indicated by a large pulse of terrestrial input at a height  
578 of 19 – 24 m) coincide with a brief interval of slightly increased foraminiferal abundance and  
579 geochemical evidence for anoxia (Figure 6). Lohali Point is another site with high sedimentation  
580 where geochemical redox proxies point towards anoxic conditions alongside the presence of  
581 benthic foraminifera. Many authors, however, favour the model of intermittent anoxia to explain  
582 these discrepancies, where faunal changes and anoxic proxies may be recording different time  
583 scales of environmental change (e.g., Simons and Kenig, 2001; Boudinot et al., 2020; Bryant et al.,  
584 2021; Forkner et al., 2021). Whilst not likely to be the sole driver for these paradoxical signals,  
585 anoxia just below the sediment-water interface is one hypothesis to explain geochemical proxy  
586 records of increased anoxia at sites with high sedimentation rates, especially when geochemical  
587 proxies are countered by micropalaeontological indicators.

### 588 **1.3.7 Photoc Zone Euxinia (PZE)**

589 Photoc zone euxinia (PZE) is a phenomenon whereby anoxia and free hydrogen sulfide extend into  
590 the shallow photic zone, and is usually related to particularly strong anoxic conditions extending  
591 from the sea-floor (Pancost et al., 2004). Isorenieratane, a marker for photic zone euxinia, was  
592 difficult to resolve in the chromatogram of the aromatic fraction, suggesting low overall

593 concentrations. As such, a crude assessment of the presence of its derivative molecules was  
594 undertaken (see Methods – Lipid biomarkers). These data broadly follow redox trends from Pr/Ph  
595 and C<sub>34</sub>/C<sub>35</sub> HH for Lohali Point, Rebecca Bounds and Pratts Landing (Figures 3, 5, 7), suggesting  
596 that PZE is linked to stronger anoxic conditions at the sea floor. Gunnison Gorge shows no  
597 variation of isorenieratane, however (Figure 4), and data from Billings Landfill show opposing  
598 trends (Figure 6). Isorenieratane derivatives are absent at Billings Landfill during lowest values of  
599 redox proxies (20.5 – 23 m height), further supporting the hypothesis of anoxic pore waters  
600 underneath an otherwise mixed and oxygenated water column. Other studies on CTB sections  
601 have noted isorenieratane derivatives within bioturbated limestone beds across the central US  
602 WIS (Simons and Kenig, 2001), and in sediments containing benthic and planktic foraminifera in  
603 southern Utah (Boudinot et al., 2020). These studies have postulated that PZE alongside faunal  
604 activity highlights the dynamic nature of redox conditions in the WIS, where intermittent anoxic  
605 events can alternate with intervals of increased oxygenation and may indicate seasonal, or other  
606 episodic, drivers of redox conditions (Boudinot et al., 2020; Forkner et al., 2021). In reality, all  
607 samples are composites of environments across a range of time, indicating the need for future  
608 studies at sedimentary lamination level.

609 Our data support low isorenieratane concentrations in all studied sections and indicate no  
610 prominent episodes of PZE. This is in contrast to Boudinot et al. (2020) who propose that elevated  
611 isorenieratane and an increase in anoxia during OAE2 at the SH#1 core in Utah is due to the site's  
612 unique depositional environment along the productive western margin. Although this core is only  
613 180 km from Lohali Point in present-day geography, during the CTB they do not exhibit similar  
614 trends in terrigenous input, stratification or redox, suggesting terrestrial influence,  
615 palaeobathymetry and oceanography may have been very different between these two sites  
616 along the western margin of the WIS.

617 On the basis of isorenieratane presence, Simons et al. (2003) suggested a more dynamic and well-  
618 mixed southern WIS compared to the less-oxygenated Canadian part of the basin. Whilst our data  
619 do not show elevated isorenieratane within the northern Pratts Landing section, elevated

620 gammacerane and TOC coupled with decreased Pr/Ph and C<sub>34</sub>/C<sub>35</sub> HH do suggest a well-stratified,  
621 anoxic environment (Figure 7).

### 622 1.3.8 Benthonic Zone (BOZ)

623 The BOZ has been identified by increased abundances of planktic and benthic foraminifera in the  
624 *Sciponoceras* biozone of Lohali Point (Leckie et al., 1998; West et al., 1998) and Billings Landfill  
625 (Dameron et al., in press). Lowery et al. (2018) propose that increased oxygen was the primary  
626 control on foraminifera abundance in the WIS, ruling out the effects of salinity, pH and water  
627 depth. Redox proxy data within this study, however, do not conclusively support oxygenation  
628 during the BOZ for these sites. This may be due to high sedimentation rates at these sites driving  
629 increased pore-water anoxia, but the limited nature of the BOZ at these sites compared to those  
630 more central in the seaway does also point to generally inhospitable conditions in the proximal  
631 realm, perhaps related to productivity-driven expansion of the OMZ (Leckie et al., 1998; Dameron  
632 et al., in press). While these findings are in agreement with that of another proximal site in Utah  
633 (Boudinot et al., 2020), where no increase in oxygenation is apparent during OAE2, they  
634 contradict those of Lowery et al. (2018) who find increased benthic foraminiferal abundances  
635 along the western proximal part of the basin. Foraminiferal analysis has not been conducted at  
636 Pratts Landing, however, despite trace amounts of planktic foraminifera in the Belle Fouche  
637 Formation of Alberta, Saskatchewan and Manitoba (McNeil and Caldwell, 1981; Bloch et al.,  
638 1999), the BOZ is not generally recognised at significant levels in Canadian sites.

639 Whilst redox proxies are not necessarily an optimal marker for the BOZ, this study shows that  
640 sterane abundance may be a more useful marker. At Lohali Point, Billings Landfill and Rebecca  
641 Bounds, the onset of the CIE (i.e., equivalent to the timing of the BOZ) is marked by a minima in  
642 C<sub>28</sub> sterane values (figures 3, 5, 6). Furthermore, an assessment of published sterane data across  
643 the WIS shows a decrease in C<sub>28</sub> sterane, or generally low values, within OAE2 is common at sites  
644 across Texas, New Mexico and Colorado (Supplemental Material F). This supports the presence of  
645 more habitable 'normal marine' waters during the BOZ without the high abundances of  
646 prasinophytes that characterise much of the CTB.



### 647    **1.3.9       Comparison of sites**

648    This study of five sites shows clear heterogeneity in terms of geochemical expressions of  
649    oceanography, redox conditions and ecological change across the WIS (Figure 13):

- 650       • Lohali Point exhibits some of the lowest, and most anoxic, redox values, yet is  
651       characterised by low prasinophyte occurrence and organic matter preservation, and  
652       diverse foraminiferal assemblages (Leckie et al., 1991). We suggest this disparity is due to  
653       particularly high sedimentation rates, enhancing burial of sediments and causing pore-  
654       waters to become anoxic, a hypothesis supported by studies of proximal sites in the  
655       Canadian WIS (Plint et al., 2012). Thus geochemical signals are enhanced by pore-water  
656       anoxia, rather than reflecting the true redox state of the water column.
- 657       • The Gunnison Gorge section does not include the CIE of OAE2 due to its location on a  
658       bathymetric high and subsequent winnowing of any sediments that may have been  
659       deposited during OAE2. The low water depths of this section are expressed by redox  
660       values suggesting a relatively oxygenated environment, with low organic matter  
661       accumulation and low TOC values.
- 662       • The most distal site here, Rebecca Bounds, has the highest levels of organic matter  
663       accumulation due its distance from clastic sediment input that would otherwise dilute  
664       organic matter.
- 665       • An oceanographic front is postulated at the Billings Landfill site, due to the decrease in  
666       stratification concurrent with an increase in water depth. This is counter to trends seen in  
667       other proximal sites in basin and suggests caballing, or at least increased water column  
668       overturning, at this site during highest sea-levels indicative of a mixing between two  
669       water masses.
- 670       • Pratts Landing is the most northerly site and exhibits vastly different trends to other sites  
671       studied here, with particularly high TOC values and geochemical proxies suggestive of  
672       very stratified, anoxic and prasinophyte-rich waters from sediments deposited during

OAE2 and beyond. This difference in geochemical signal suggests a vastly different oceanographic regime, and further supports the presence of a Boreal-Tethyan oceanographic front between Canada and the US – potentially in the proximity of the Billings Landfill site.

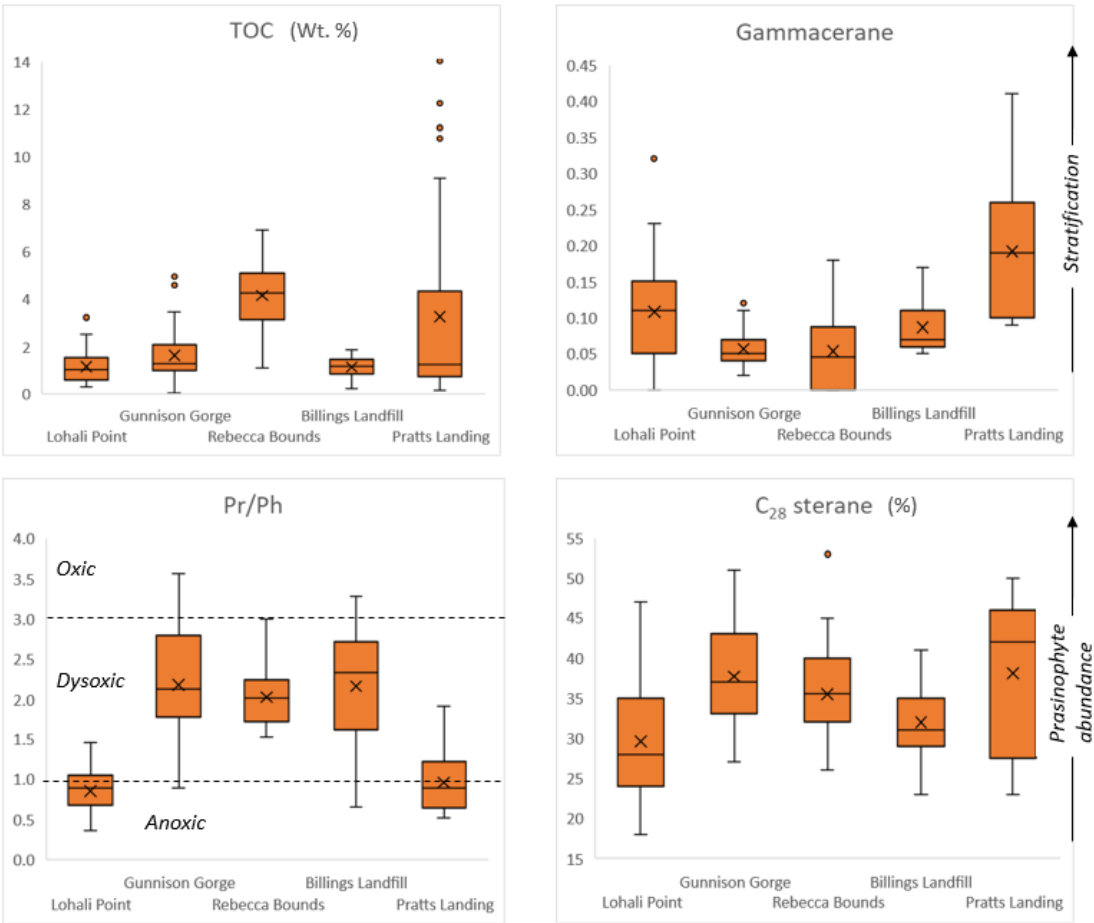


**Figure 13: Box and whisker diagrams showing data distribution for four key oceanographic proxies across all five sites: TOC, Gammacerane (Gammacerane/(gammacerane + C<sub>30</sub> αβ hopane): stratification proxy) , Pristane/Phytane (redox proxy) and C<sub>28</sub> sterane (C<sub>28</sub> steranes / Σ(C<sub>27-29</sub> steranes) \* 100: prasinophyte proxy). Line within the box indicates median, cross within the box indicates the mean. See Table 1 for more information on geochemical proxies.**

### 1.4 Conclusions (376)

Environmental conditions across the mid-Cretaceous OAE2 within the five sites studied here (Lohali Point, Gunnison Gorge, Rebecca Bounds, Billings Landfill and Pratts Landing) show clear

687 differences, indicating heterogeneity and complexity in the drivers resulting in anoxia,  
688 stratification and organic matter deposition across the basin.

689 Despite these differences, trends among geochemical proxies can be demonstrated. At most sites  
690 (Lohali Point, Gunnison Gorge and Pratts Landing) stratification appears to lead to low-oxygen  
691 conditions, driven by increased water depths allowing a more stable chemocline to develop. In  
692 addition to water depth, stratification can be locally enhanced by increases in low-density  
693 freshwater run-off in the upper water column. At Billings Landfill, however, a breakdown in  
694 stratification occurs during increased water depths, suggesting caballing and the local presence of  
695 the mixing front between Boreal and Tethyan waters.

696 The C<sub>28</sub> sterane has been shown to be a useful proxy for presence of prasinophyte algae.  
697 Prasinophyte-rich algal productivity is evident at every site, driven by increased stratification and  
698 possibly linked to perturbations of the marine biogeochemical cycle, such as the increase of  
699 ammonium nitrogen sources.

700 Evidence for prasinophyte dominance decreases at the onset of OAE2 for sites within the US part  
701 of the WIS, concurrent with the presence of the BOZ. An increase in oxygenation is not always  
702 identified at the BOZ in proximal sites, due to the influence of high terrigenous sedimentation,  
703 pore-water anoxia and/or enhanced nutrient-driven productivity. We show that sterane ratios are  
704 a more reliable geochemical proxy for assessing changes in faunal communities and identifying  
705 the presence of the BOZ.

706 Intermittent dysoxia/oxic conditions allowed benthos to exist on the sea floor, in some cases in  
707 beds that contain evidence for anoxia and PZE. In addition to this, we propose that pore-water  
708 anoxia, occurring where there is particularly high sedimentation rates along the western part of  
709 the WIS, can enhance the anoxic signal in sediments accumulating beneath a well-oxygenated  
710 water column. Proximal sites show differing trends to the Rebecca Bounds core which is located  
711 more centrally in the basin.

712 This study is one example of how a multidisciplinary approach based on several different  
713 indicators and proxies can facilitate the disentanglement of seemingly conflicting data sets,  
714 leading to a more robust assessment of environmental conditions captured in ancient sediments  
715 across extreme episodes.

## 716 **1.5 Declaration of competing interest**

717 The authors declare that they have no known competing financial interests or personal  
718 relationships that could have appeared to influence the work reported in this paper.

## 719 **1.6 Author contributions**

720 LJR designed the study; LJR, JL and SM logged and obtained samples for Gunnison Gorge; LJR and  
721 KSG generated isotopic, elemental, lipid biomarker and palynofacies data; ICH and JEAM assisted  
722 with palynological preparation and interpretation; PB generated nannofossil data; CPF conducted  
723 PCA statistics. DRG generated isotopic data, and NAGMvH and NMP generated palynofacies data,  
724 for Pratts Landing. RML provided samples for Lohali Point and Billings Landfill and contributed  
725 valuable scientific input, SD provided analysis for the Billings Landfill site. LJR wrote the  
726 manuscript with editorial support from JHW, and all co-authors.

727

## 728 **1.7 Acknowledgements**

729 LJR acknowledges support from the Natural Environmental Research Council UK (NE/L002531/1),  
730 AAPG Foundation Grant-in-Aid (Marta S. Weeks Named Grant) and Geological Society of London  
731 Research Grant (William George Fearnside's fund). Samples were generously donated by Mark  
732 Leckie (Lohali Point and Billings Landfill), Guy Plint (Pratts Landing) and the USGS Core Research  
733 Centre (Rebecca Bounds). Samples from Lohali Point originate from Navajo and Hopi ancestral  
734 lands. CPF acknowledges CIRA grant CIRA-2019-066.

## 735    **1.8    References**

- 736    Allison, P., Wells, M., 2006. Circulation in large ancient epicontinental seas: What was different  
737    and why? *Palaios* 21, 513–515.
- 738    Arthur, M.A., Sageman, B.B., 2005. Sea Level Control on Source Rock Development: Perspectives  
739    from the Holocene Black Sea, the mid-Cretaceous Western Interior Basin of North America, and  
740    the Late Devonian Appalachian Basin, in: Harris, N.B. (Ed.), *The Deposition of Organic Carbon-Rich*  
741    *Sediments: Models, Mechanisms and Consequences*. SEPM.
- 742    Banta, A.B., Wei, J.H., Welander, P.V., 2015. A distinct pathway for tetrahymanol synthesis in  
743    bacteria. *Proceedings of the National Academy of Sciences* 112, 13478–13483.
- 744    Baranyi, V., Pálfi, J., Görög, Á., Riding, J.B., Raucsik, B., 2016. Multiphase response of  
745    palynomorphs to the Toarcian Oceanic Anoxic Event (Early Jurassic) in the Réka Valley section,  
746    Hungary. *Review of Palaeobotany and Palynology* 235, 51–70.
- 747    Barnosky, A.D., Matzke, N., Tomiya, S., Wogan, G.O.U., Swartz, B., Quental, T.B., Marshall, C.,  
748    McGuire, J.L., Lindsey, E.L., Maguire, K.C., Mersey, B., Ferrer, E.A., 2011. Has the Earth's sixth mass  
749    extinction already arrived? *Nature* 471, 51–57.
- 750    Bhattacharya, J.P., Tye, R.S., 2004. Searching for Modern Ferron Analogs and Application to  
751    Subsurface Interpretation. doi:10.1306/St50983
- 752    Bloch, J.D., Schröder-Adams, C.J., Leckie, D.A., Craig, J., McIntyre, D.J., 1999. Sedimentology,  
753    micropalaeontology, geochemistry and hydrocarbon potential of shale from the cretaceous lower  
754    Colorado group in Western Canada (No. 531), Geological Survey of Canada, Bulletin.
- 755    Boudinot, F.G., Dildar, N., Leckie, R.M., Parker, A., Jones, M.M., Sageman, B.B., Bralower, T.J.,  
756    Sepúlveda, J., 2020. Neritic ecosystem response to Oceanic Anoxic Event 2 in the Cretaceous  
757    Western Interior Seaway, USA. *Palaeogeography, Palaeoclimatology, Palaeoecology* 546, 109673.
- 758    Bralower, T.J., Bergen, J.A., 1998. Cenomanian-Santonian Calcareous Nannofossil Biostratigraphy  
759    of a Transect of Cores Drilled Across the Western Interior Seaway. doi:10.2110/csp.98.06.0059
- 760    Breitburg, D., Levin, L.A., Oschlies, A., Grégoire, M., Chavez, F.P., Conley, D.J., Garçon, V., Gilbert,  
761    D., Gutiérrez, D., Isensee, K., Jacinto, G.S., Limburg, K.E., Montes, I., Naqvi, S.W.A., Pitcher, G.C.,  
762    Rabalais, N.N., Roman, M.R., Rose, K.A., Seibel, B.A., Telszewski, M., Yasuhara, M., Zhang, J., 2018.  
763    Declining oxygen in the global ocean and coastal waters. *Science* 359, eaam7240.
- 764    Bryant, R., Leckie, M.R., Bralower, T.J., Jones, M.M. and Sageman B.B. (2021) Microfossil and  
765    geochemical records reveal high-productivity palaeoenvironments in the Cretaceous Western

766 Interior Seaway during Oceanic Anoxic Event 2. *Palaeogeography, Palaeoclimatology,*  
 767 *Palaeoecology* 584, 110679, <https://doi.org/10.1016/j.palaeo.2021.110679>

768 Caldwell, W.G.E., Diner, R., Eicher, D.G., Fowler, S.P., North, B.R., Stelck, C.R., von Holdt Wilhelm,  
 769 L., 1993. Foraminiferal biostratigraphy of Cretaceous marine cyclothem, in: Caldwell, W.G.E.,  
 770 Kauffman, E.G. (Eds.), *Evolution of the Western Interior Basin*. Geological Association of Canada,  
 771 pp. 477–520.

772 Ceballos, G., Ehrlich, P.R., Dirzo, R., 2017. Biological annihilation via the ongoing sixth mass  
 773 extinction signaled by vertebrate population losses and declines. *Proceedings of the National*  
 774 *Academy of Sciences* 114, E6089–E6096.

775 Chinn, E.W., 1991. The role of organic geochemistry in petroleum exploration. *Basin Research*  
 776 *Institute Bulletin*, Louisiana State University, Baton Rouge 15–23.

777 Cochlan, W., Harrison, P., 1991. Uptake of nitrate, ammonium, and urea by nitrogen-starved  
 778 cultures of *Micromonas pusilla* (Prasinophyceae): Transient responses. *Journal of Phycology* 27,  
 779 673–679.

780 Cronin, S.J., Neall, V.E., Lecointre, J.A., Hedley, M.J., Loganathan, P., 2003. Environmental hazards  
 781 of fluoride in volcanic ash: a case study from Ruapehu volcano, New Zealand. *Journal of*  
 782 *Volcanology and Geothermal Research* 121, 271–291.

783 Curiale, J.A., 1994a. High-Resolution Organic Record of Bridge Creek Deposition, Northwest New-  
 784 Mexico. *Organic Geochemistry* 21, 489–507.

785 Curiale, J.A., 1994b. Geochemical Anomalies at the Cenomanian-Turonian Boundary, Northwest  
 786 New-Mexico. *Organic Geochemistry* 22, 487–500.

787

788 Dameron, S.N., Leckie, R.M., Polyak, D.E., Robinson, L.J., Whiteside, J.H., Elder, W.P., Leithold, E.L.,  
 789 Tibert, N.E., in press. A Palaeoceanographic Divide in the Western Interior Seaway during the  
 790 Cenomanian-Turonian OAE2. *Micropalaeontology*.

791 Dickson, A.J., Jenkyns, H.C., Porcelli, D., van den Boorn, S., Idiz, E., 2016a. Basin-scale controls on  
 792 the molybdenum-isotope composition of seawater during Oceanic Anoxic Event 2 (Late  
 793 Cretaceous). *Geochimica et Cosmochimica Acta* 178, 291–306.

794 Dickson, A.J., Jenkyns, H.C., Porcelli, D., van den Boorn, S., Idiz, E., Owens, J.D., 2016b.  
 795 Corrigendum to “Basin-scale controls on the molybdenum-isotope composition of seawater  
 796 during Oceanic Anoxic Event 2 (Late Cretaceous)” [*Geochim. Cosmochim. Acta* 178 (2016) 291–  
 797 306]. *Geochimica et Cosmochimica Acta* 189, 404–405.

798 Didyk, B.M., Simoneit, B.R.T., Brassell, S.C., Eglinton, G., 1978. Organic Geochemical Indicators of  
799 Palaeo-Environmental Conditions of Sedimentation. *Nature* 272, 216–222.

800 Dionne, D., Schroder-Adams, C., Cumbaa, S., 2016. Foraminiferal response to Ecological  
801 perturbations along the eastern margin of the Canadian Western Interior seaway, Cenomanian-  
802 Turonian interval. *The Journal of Foraminiferal Research* 46, 124–148.

803 Dirzo, R., Young, H.S., Galetti, M., Ceballos, G., Isaac, N.J.B., Collen, B., 2014. Defaunation in the  
804 Anthropocene. *Science* 345, 401–406.

805 Dougherty, R.C., Strain, H.H., Svec, W.A., Uphaus, R.A., Katz, J.J., 1970. Structure, properties, and  
806 distribution of chlorophyll c. *Journal of the American Chemical Society* 92, 2826–2833.

807 Du Vivier, A.D.C., Selby, D., Sageman, B.B., Jarvis, I., Gröcke, D.R. & Voigt, S. (2014). Marine  
808 187Os/188Os isotope stratigraphy reveals the interaction of volcanism and ocean circulation  
809 during Oceanic Anoxic Event 2. *Earth & Planetary Science Letters* 389:23–33.  
810 <https://doi.org/10.1016/j.epsl.2013.12.024>

811 Eicher, D.L., Diner, R., 1985. Foraminifera as Indicators of Water Mass in the Cretaceous  
812 Greenhorn Sea, Western Interior, in: Pratt, L.M., Kauffman, E.G., Zelt, F.B. (Eds.), *Fine-Grained  
813 Deposits and Biofacies of the Cretaceous Western Interior Seaway*. SEPM Society for Sedimentary  
814 Geology, Tulsa, OK, pp. 60–71.

815 Eicher, D.L., Worstell, P., 1970. Cenomanian and Turonian Foraminifera from the Great Plains,  
816 United States. *Micropalaeontology* 16, 269–324.

817 Elder, W.P., 1987. The Palaeoecology of the Cenomanian-Turonian (Cretaceous) Stage Boundary  
818 Extinctions at Black Mesa, Arizona. *Palaios* 2, 24–40.

819 Elder, W.P., Kirkland, J.I., 1993. Cretaceous palaeogeography of the Colorado Plateau and  
820 adjacent areas, in: *Aspects of Mesozoic Geology and Palaeontology of the Colorado Plateau  
821 Region*, Museum of Northern Arizona Bulletin. pp. 129–151.

822 Elderbak, K., Leckie, R.M., 2016. Palaeocirculation and foraminiferal assemblages of the  
823 Cenomanian-Turonian Bridge Creek Limestone bedding couplets: Productivity vs. dilution during  
824 OAE2. *Cretaceous Research* 60, 52–77.

825 Elderbak, K., Leckie, R.M., Tibert, N.E., 2014. Palaeoenvironmental and palaeoceanographic  
826 changes across the Cenomanian–Turonian Boundary Event (Oceanic Anoxic Event 2) as indicated  
827 by foraminiferal assemblages from the eastern margin of the Cretaceous Western Interior Sea.  
828 *Palaeogeography, Palaeoclimatology, Palaeoecology* 413, 29–48.

829 Eldrett, J.S., Dodsworth, P., Bergman, S.C., Wright, M., Minisini, D., 2017. Water-mass evolution in  
830 the Cretaceous Western Interior Seaway of North America and equatorial Atlantic. *Climate of the*  
831 *Past* 13, 855–878.

832 Eldrett, J.S., Minisini, D., Bergman, S.C., 2014. Decoupling of the carbon cycle during Ocean Anoxic  
833 Event 2. *Geology* 42, 567–570.

834 Erbacher, J., Huber, B.T., Norris, R.D., Markey, M., 2001. Increased thermohaline stratification as a  
835 possible cause for an ocean anoxic event in the Cretaceous period. *Nature* 409, 325–327.

836 Fisher, C.G., Hay, W.W., Eicher, D.L., 1994. Oceanic Front in the Greenhorn Sea (Late Middle  
837 through Late Cenomanian). *Palaeoceanography* 9, 879–892.

838 Floegel, S., Hay, W.W., DeConto, R.M., Balukhovsk, A.N., 2005. Formation of sedimentary bedding  
839 couplets in the Western Interior Seaway of North America - implications from climate system  
840 modeling. *Palaeogeography Palaeoclimatology Palaeoecology* 218, 125–143.

841 Floegel, S., 2001. On the influence of precessional Milankovitch cycles on the Late Cretaceous  
842 climate system: comparison of GCM-results, geochemical, and sedimentary proxies for the  
843 Western Interior Seaway of North America. Christian-Albrechts-University.

844 Forkner, R.M., Dahl, J., Fildani, A., Barbanti, S.M., Yurchenko, I.A., Moldowan, J.M., 2021. Anatomy  
845 of an extinction revealed by molecular fossils spanning OAE2. *Scientific Reports* 11, 13621.

846 French, K.L., Birdwell, J.E., Whidden, K.J., 2019. Geochemistry of a thermally immature Eagle Ford  
847 Group drill core in central Texas. *Organic Geochemistry* 131, 19–33.

848 Furmann, A., Mastalerz, M., Brassell, S.C., Pedersen, P.K., Zajac, N.A., Schimmelmann, A., 2015.  
849 Organic matter geochemistry and petrography of Late Cretaceous (Cenomanian-Turonian)  
850 organic-rich shales from the Belle Fourche and Second White Specks formations, west-central  
851 Alberta, Canada. *Organic Geochemistry* 85, 102–120.

852 Gale, A.S., Voigt, S., Sageman, B.B., Kennedy, W.J., 2008. Eustatic sea-level record for the  
853 Cenomanian (Late Cretaceous)—Extension to the Western Interior Basin, USA. *Geology* 36, 859.

854 Grice, K., Schaeffer, P., Schwark, L., Maxwell, J. R., Molecular indicators of palaeoenvironmental  
855 conditions in an immature Permian shale (Kupferschiefer, Lower Rhine Basin, north-west  
856 Germany) from free and S-bound lipids. *Organic Geochemistry*, 25(3/4), pp. 131-147

857 Hancock, J.M., Kauffman, E.G., 1979. The great transgressions of the Late Cretaceous. *Journal of*  
858 *the Geological Society* 136, 175–186.



859 Hawkins, E., Ortega, P., Suckling, E., Schurer, A., Hegerl, G., Jones, P., Joshi, M., Osborn, T.J.,  
860 Masson-Delmotte, V., Mignot, J., Thorne, P., Oldenborgh, G.J. van, 2017. Estimating Changes in  
861 Global Temperature since the Preindustrial Period. *Bulletin of the American Meteorological*  
862 *Society* 98, 1841–1856.

863 Hay, M.J., Plint, A.G., 2020. High-frequency sequences within a retrogradational deltaic  
864 succession: Upper Cenomanian Dunvegan Formation, Western Canada Foreland Basin. *The*  
865 *Depositional Record* 6, 524–551.

866 Hay, W.W., Eicher, D., Diner, L., 1993. Physical oceanography and water masses of the Cretaceous  
867 Western Interior Seaway, in: Caldwell W. G. E.; Kauffman, E.G. (Ed.), *Evolution of the Western*  
868 *Interior Basin*. Geological Association of Canada, pp. 297–318.

869 Higgins, M.B., Robinson, R.S., Husson, J.M., Carter, S.J., Pearson, A., 2012. Dominant eukaryotic  
870 export production during ocean anoxic events reflects the importance of recycled NH<sub>4</sub><sup>+</sup>.  
871 *Proceedings of the National Academy of Sciences* 109, 2269–2274.

872 Hinsbergen, D.J.J. van, Groot, L.V. de, Schaik, S.J. van, Spakman, W., Bijl, P.K., Sluijs, A., Langereis,  
873 C.G., Brinkhuis, H., 2015. A Palaeolatitude Calculator for Palaeoclimate Studies. *PLOS ONE* 10,  
874 e0126946.

875 IPCC, 2021. *Climate Change 2021: The Physical Science Basis*. Contribution of Working Group I to  
876 the Sixth Assessment Report of the Intergovernmental Panel on Climate Change. Cambridge  
877 University Press.

878 Jarvis, I., Lignum, J.S., Gröcke, D.R., Jenkyns, H.C. & Pearce, M.A. (2011). Black shale deposition,  
879 atmospheric CO<sub>2</sub> drawdown and cooling during the Cenomanian–Turonian Oceanic Anoxic Event.  
880 *Palaeoceanography* 26:PA3201. <https://doi.org/10.1029/2010PA002081>

881 Jenkyns, H.C., 1980. Cretaceous anoxic events: from continents to oceans. *Journal of the*  
882 *Geological Society* 137, 171–188.

883 Jenkyns, H.C., 2003. Evidence for rapid climate change in the Mesozoic-Palaeogene greenhouse  
884 world. *Philosophical Transactions of the Royal Society a-Mathematical Physical and Engineering*  
885 *Sciences* 361, 1885–1916.

886 Jenkyns, H.C., 2010. Geochemistry of oceanic anoxic events. *Geochemistry Geophysics*  
887 *Geosystems* 11. doi:Artn Q03004 10.1029/2009gc002788

888 Joo, Y.J., Sageman, B.B., 2014. Cenomanian to Campanian Carbon Isotope Chemostratigraphy  
889 from the Western Interior Basin, USA. *Journal of Sedimentary Research* 84, 529–542.

890 Kauffman, E.G., 1984. Palaeobiogeography and evolutionary response dynamic in the Cretaceous  
 891 Western Interior Seaway of North America, in: Westerman, G.E.G. (Ed.), Jurassic-Cretaceous  
 892 Biochronology and Palaeogeography of North America. Geological Association of Canada, pp.  
 893 273–306.

894 Kauffman, W.G.E., Caldwell, W.G., 1993. The Western Interior Basin in Space and Time, in:  
 895 Evolution of the Western Interior Basin. Geological Association of Canada, pp. 1–30.

896 Keeling, R.E., Körtzinger, A., Gruber, N., 2010. Ocean deoxygenation in a warming world. Annual  
 897 Review of Marine Science 2, 199–229.

898 Keller, G., Pardo, A., 2004. Age and palaeoenvironment of the Cenomanian-Turonian global  
 899 stratotype section and point at Pueblo, Colorado. Marine Micropalaeontology 51, 95–128.

900 Kidder, D.L., Worsley, T.R., 2010. Phanerozoic Large Igneous Provinces (LIPs), HEATT (Haline  
 901 Euxinic Acidic Thermal Transgression) episodes, and mass extinctions. Palaeogeography  
 902 Palaeoclimatology Palaeoecology 295, 162–191.

903 Kirkland, J.I., 1991. Lithostratigraphic and biostratigraphic framework for the Mancos Shale (Late  
 904 Cenomanian to Middle Turonian) at Black Mesa, northeastern Arizona, in: Nations, J.G., J.D.,  
 905 Eaton (Ed.), Stratigraphy, Depositional Environments, and Sedimentary Tectonics of the Western  
 906 Margin, Cretaceous Western Interior Seaway. Geological Society of America.

907 Kirkland, J.I., 1996. Palaeontology of the Greenhorn cyclothem (Cretaceous: Late Cenomanian to  
 908 Middle Turonian) at Black Mesa, northeastern Arizona. New Mexico Museum of Natural History.

909 Koopmans, M.P., Köster, J., Van Kaam-Peters, H.M.E., Kenig, F., Schouten, S., Hartgers, W.A., de  
 910 Leeuw, J.W., Sinninghe Damsté, J.S., 1996. Diagenetic and catagenetic products of isorenieratene:  
 911 Molecular indicators for photic zone anoxia. Geochimica et Cosmochimica Acta 60, 4467–4496.

912 Kump, L.R., Slingerland, R.L., 1999. Circulation and stratification of the early Turonian Western  
 913 Interior Seaway: Sensitivity to a variety of forcings, in: Evolution of the Cretaceous Ocean-Climate  
 914 System. Geological Society of America. doi:10.1130/0-8137-2332-9.181

915 Kuroda, J., Ogawa, N.O., Tanimizu, M., Coffin, M.F., Tokuyama, H., Kitazato, H., Ohkouchi, N.,  
 916 2007. Contemporaneous massive subaerial volcanism and late cretaceous Oceanic Anoxic Event 2.  
 917 Earth and Planetary Science Letters 256, 211–223.

918 Leckie, R.M., Bralower, T.J., Cashman, R., 2002. Oceanic anoxic events and plankton evolution:  
 919 Biotic response to tectonic forcing during the mid-Cretaceous. Palaeoceanography 17. doi:Artn  
 920 1041 10.1029/2001pa000623

- 921 Leckie, R.M., Schmidt, M.G., Finkelstein, D., Yuretich, R., 1991. Palaeoceanographic and  
922 palaeoclimatic interpretations of the Mancos Shale (Upper Cretaceous), Black Mesa Basin,  
923 Arizona, in: Nations, J.G., J.D.; Eaton (Ed.), *Stratigraphy, Depositional Environments, and*  
924 *Sedimentary Tectonics of the Western Margin, Cretaceous Western Interior Seaway*, Special  
925 Paper 260. Geological Society of America, pp. 139–152.
- 926 Leckie, R.M., Yuretich, R.F., West, O.L.O., Finkelstein, D., Schmidt, M., 1998. Palaeoceanography of  
927 the Southwestern Western Interior Sea During the Time of the Cenomanian-Turonian Boundary  
928 (Late Cretaceous), in: Dean, W.E., Arthur, M.A. (Eds.), *Stratigraphy and Palaeoenvironments of the*  
929 *Cretaceous Western Interior Seaway, USA*. SEPM (Society for Sedimentary Geology).  
930 doi:10.2110/csp.98.06
- 931 Leithold, E.L., 1993. Preservation of laminated shale in ancient clinoforms; comparison to modern  
932 subaqueous deltas. *Geology* 21, 359–362.
- 933 Li, R.W., 1989. Geological Occurrence and Its Palaeoenvironmental Significance of Gammacerane.  
934 *Chinese Science Bulletin* 34, 1208–1211.
- 935 Li, Z., Bhattacharya, J., Schieber, J., 2015. Evaluating along-strike variation using thin-bedded  
936 facies analysis, Upper Cretaceous Ferron Notom Delta, Utah. *Sedimentology* 62, 2060–2089.
- 937 Litchman, E., Klausmeier, C.A., Miller, J.R., Schofield, O.M., Falkowski, P.G., 2006. Multi-nutrient,  
938 multi-group model of present and future oceanic phytoplankton communities 22.
- 939 Lowery, C.M., Leckie, R.M., Bryant, R., Elderbak, K., Parker, A., Polyak, D.E., Schmidt, M.,  
940 Snoeyenbos-West, O., Sterzinar, E., 2018. The Late Cretaceous Western Interior Seaway as a  
941 model for oxygenation change in epicontinental restricted basins. *Earth-Science Reviews* 177,  
942 545–564.
- 943 Lowery, Cunningham, R., Barrie, C.D., Bralower, T., Snedden, J.W., 2017. The Northern Gulf of  
944 Mexico During OAE2 and the Relationship Between Water Depth and Black Shale Development.  
945 *Palaeoceanography* 32, 1316–1335.
- 946 McNeil, D.H., Caldwell, W.G.E., 1981. Cretaceous Rocks and Their Foraminifera in the Manitoba  
947 Escarpment, The Geological Association Of Canada Special Paper 21. The Geological Association  
948 Of Canada.
- 949 Merewether, E.A., Cobban, W.A., 1986. Biostratigraphic Units and Tectonism in the Mid-  
950 Cretaceous Foreland of Wyoming, Colorado, and Adjoining Areas. doi:10.1306/M41456C21
- 951 Moldowan, J.M., Dahl, J., Huizinga, B.J., Fago, F.J., Hickey, L.J., Peakman, T.M., Taylor, D.W., 1994.  
952 The Molecular Fossil Record of Oleanane and Its Relation to Angiosperms. *Science* 265, 768–771.

953 Monteiro, F.M., Pancost, R.D., Ridgwell, A., Donnadieu, Y., 2012. Nutrients as the dominant  
 954 control on the spread of anoxia and euxinia across the Cenomanian-Turonian oceanic anoxic  
 955 event (OAE2): Model-data comparison. *Palaeoceanography* 27. doi:10.1029/2012PA002351

956 Naafs, B.D.A., Monteiro, F.M., Pearson, A., Higgins, M.B., Pancost, R.D., Ridgwell, A., 2019.  
 957 Fundamentally different global marine nitrogen cycling in response to severe ocean  
 958 deoxygenation. *Proceedings of the National Academy of Sciences* 116, 24979–24984.

959 O’Brien, C.L., Robinson, S.A., Pancost, R.D., Damste, J.S.S., Schouten, S., Lunt, D.J., Alsenz, H.,  
 960 Bomemann, A., Bottini, C., Brassell, S.C., Farnsworth, A., Forster, A., Huber, B.T., Inglis, G.N.,  
 961 Jenkyns, H.C., Linnert, C., Littler, K., Markwick, P., McAnena, A., Mutterlose, J., Naafs, B.D.A.,  
 962 Puttmann, W., Sluijs, A., van Helmond, N.A.G.M., Vellekoop, J., Wagner, T., Wrobel, N.E., 2017.  
 963 Cretaceous sea-surface temperature evolution: Constraints from TEX86 and planktonic  
 964 foraminiferal oxygen isotopes. *Earth-Science Reviews* 172, 224–247.

965 Ostrander, C.M., Owens, J.D., Nielsen, S.G., 2017. Constraining the rate of oceanic deoxygenation  
 966 leading up to a Cretaceous Oceanic Anoxic Event (OAE2: ~94 Ma). *Science Advances* 3, e1701020.

967 Owens, J.D., Gill, B.C., Jenkyns, H.C., Bates, S.M., Severmann, S., Kuypers, M.M.M., Woodfine,  
 968 R.G., Lyons, T.W., 2013. Sulfur isotopes track the global extent and dynamics of euxinia during  
 969 Cretaceous Oceanic Anoxic Event 2. *Proceedings of the National Academy of Sciences* 110, 18407–  
 970 18412.

971 Pancost, M.A., Freeman, K.H., Arthur, M.A., 1998. Organic Geochemistry of the Cretaceous  
 972 Western Interior Seaway: A Trans-Basinal Evaluation. *SEPM Concepts in Sedimentology and*  
 973 *Palaeontology* 6, 173–188.

974 Pancost, R.D., Crawford, N., Magness, S., Turner, A., Jenkyns, H.C., Maxwell, J.R., 2004. Further  
 975 evidence for the development of photic-zone euxinic conditions during Mesozoic oceanic anoxic  
 976 events. *Journal of the Geological Society* 161, 353–364.

977 Parker, A.L., 2016. Oceanic Anoxia Event 2 (~94 Ma) in the U.S. Western Interior Sea: High  
 978 Resolution Foraminiferal Record of the development of anoxia in a shallow epicontinental sea.  
 979 University of Massachusetts Amherst.

980 Peters, C.C., Walters, C., Moldowan, J.M., 2005. The Biomarker Guide: Volume II. Biomarkers and  
 981 Isotopes in Petroleum Systems and Earth History. Cambridge University Press.

982 Piper, D.Z., Calvert, S.E., 2009. A marine biogeochemical perspective on black shale deposition.  
 983 *Earth-Science Reviews* 95, 63–96.

984 Plint, A.G., 2000. Sequence stratigraphy and palaeogeography of a Cenomanian deltaic complex:  
 985 the Dunvegan and lower Kaskapau formations in subsurface and outcrop, Alberta and British  
 986 Columbia, Canada. *Bulletin of Canadian Petroleum Geology* 48, 43–79.

987 Plint, A.G., Macquaker, J.H.S., Varban, B.L., 2012. Bedload Transport of Mud Across A Wide,  
 988 Storm-Influenced Ramp: Cenomanian–Turonian Kaskapau Formation, Western Canada Foreland  
 989 Basin. *BEDLOAD TRANSPORT OF MUD ACROSS A STORM-INFLUENCED CRETACEOUS RAMP. Journal*  
 990 *of Sedimentary Research* 82, 801–822.

991 Pratt, L.M., 1985. Isotopic Studies of Organic Matter and Carbonate in Rocks of the Greenhorn  
 992 Marine Cycle. doi:10.2110/sepmfg.04.038

993 Pratt, L.M., Threlkeld, C.N., 1984. Stratigraphic significance of  $^{13}\text{C}/^{12}\text{C}$  ratios in mid-Cretaceous  
 994 rocks of the western interior, U.S.A., in: *Mesozoic of Middle North America*. Canadian Society  
 995 Petroleum Geologists, pp. 305–312.

996 Prauss, M.L., 2007. Availability of Reduced Nitrogen Chemospecies in Photic-Zone Waters as the  
 997 Ultimate Cause for Fossil Prasinophyte Prosperity. *PALAIOS* 22, 489–499.

998 Riva, A., Caccialanza, P.G., Quagliaroli, F., 1988. Recognition of  $18\beta$  (H)oleanane in several crudes  
 999 and Tertiary-Upper Cretaceous sediments. Definition of a new maturity parameter. *Organic*  
 1000 *Geochemistry, Proceedings of the 13th International Meeting on Organic Geochemistry* 13, 671–  
 1001 675.

1002 Robinson, S.A., Heimhofer, U., Hesselbo, S.P., Petrizzo, M.R., 2017. Mesozoic climates and oceans  
 1003 - a tribute to Hugh Jenkyns and Helmut Weissert. *Sedimentology* 64, 1–15.

1004 Sageman, B.B., 1996. Lowstand tempestites: Depositional model for Cretaceous skeletal  
 1005 limestones, Western Interior basin. *Geology* 24, 888–892.

1006 Sageman, B.B., Arthur, M.A., 1994. Early Turonian palaeogeography/palaeobathymetric map,  
 1007 Western Interior, U.S., in: Caputo, M.V., Peterson, J.A., Franczyk, K.J. (Eds.), *Mesozoic Systems of*  
 1008 *the Rocky Mountain Region, USA, SEPM, Rocky Mountain Section*. SEPM, pp. 457–470.

1009 Sageman, B.B., Meyers, S.R., Arthur, M.A., 2006. Orbital time scale and new C-isotope record for  
 1010 Cenomanian-Turonian boundary stratotype. *Geology* 34, 125–128.

1011 Savrda, C.E., 1998. Ichnology of the Bridge Creek Limestone: Evidence for Temporal and Spatial  
 1012 Variations in Palaeo-Oxygenation in the Western Interior Seaway. doi:10.2110/csp.98.06.0127

1013 Schlanger, S.O., Arthur, M.A., Jenkyns, H.C., Scholle, P.A., 1987. The Cenomanian-Turonian  
1014 Oceanic Anoxic Event, I. Stratigraphy and distribution of organic carbon-rich beds and the Marine  
1015 delta 13C excursion. *Marine petroleum source rocks*.

1016 Schlanger, S.O., Jenkyns, H.C., 1976. Cretaceous Oceanic Anoxic Events: Causes and  
1017 Consequences. *Geologie en Mijnbouw* 55, 179–184.

1018 Schmidtko, S., Stramma, L., Visbeck, M., 2017. Decline in global oceanic oxygen content during the  
1019 past five decades. *Nature* 542, 335–+.

1020 Schröder-Adams, C., 2014. The Cretaceous Polar and Western Interior seas: palaeoenvironmental  
1021 history and palaeoceanographic linkages. *Sedimentary Geology* 301, 26–40.

1022 Schröder-Adams, C.J., Cumbaa, S.L., Bloch, J., Leckie, D.A., Craig, J., El-Dein, S.A.S., Simons,  
1023 D.J.H.A.E., Kenig, F., 2001. Late Cretaceous (Cenomanian to Campanian) palaeoenvironmental  
1024 history of the Eastern Canadian margin of the Western Interior Seaway: bonebeds and anoxic  
1025 events. *Palaeogeography Palaeoclimatology Palaeoecology* 170, 261–289.

1026 Schröder-Adams, C.J., Herrle, J.O., Tu, Q., 2012. Albian to Santonian carbon isotope excursions  
1027 and faunal extinctions in the Canadian Western Interior Sea: Recognition of eustatic sea-level  
1028 controls on a forebulge setting. *Sedimentary Geology* 281, 50–58.

1029 Schröder-Adams, C.J., Leckie, D.A., Bloch, J., Craig, J., McIntyre, D.J., Adams, P.J., 1996.  
1030 Palaeoenvironmental changes in the Cretaceous (Albian to Turonian) Colorado Group of western  
1031 Canada: Microfossil, sedimentological and geochemical evidence. *Cretaceous Research* 17, 311–  
1032 365.

1033 Schwark, L., Empt, P., 2006. Sterane biomarkers as indicators of palaeozoic algal evolution and  
1034 extinction events. *Palaeogeography, Palaeoclimatology, Palaeoecology, Evolution of the System*  
1035 *Earth in the Late Palaeozoic: Clues from Sedimentary Geochemistry* 240, 225–236.

1036 Scott, J.A., R.W.; Franks, P.C.; Evetts, M.J.; Bergen, J.A.; Stein, 1998. Timing of mid-Cretaceous  
1037 relative sea level changes in the Western Interior: Amoco No. 1 Bounds Core. *SEPM Concepts in*  
1038 *Sedimentology and Palaeontology* 6, 11–34.

1039 Simons, D.J.H., Kenig, F., 2001. Molecular fossil constraints on the water column structure of the  
1040 Cenomanian-Turonian Western Interior Seaway, USA. *Palaeogeography Palaeoclimatology*  
1041 *Palaeoecology* 169, 129–152.

1042 Simons, D.J.H., Kenig, F., Schroder-Adams, C.J., 2003. An organic geochemical study of  
1043 Cenomanian-Turonian sediments from the Western Interior Seaway, Canada. *Organic*  
1044 *Geochemistry* 34, 1177–1198.

- 1045 Sinninghe Damsté, J.S., Kenig, F., Koopmans, M.P., Köster, J., Schouten, S., Hayes, J.M., de Leeuw,  
1046 J.W., 1995. Evidence for gammacerane as an indicator of water column stratification. *Geochimica*  
1047 *et Cosmochimica Acta* 59, 1895–1900.
- 1048 Slingerland, R., Kump, L.R., Arthur, M.A., Fawcett, P.J., Sageman, B.B., Barron, E.J., 1996. Estuarine  
1049 circulation in the Turonian Western Interior seaway of North America. *Geological Society of*  
1050 *America Bulletin* 108, 941–952.
- 1051 Sun, X., Zhang, T., Sun, Y., Milliken, K.L., Sun, D., 2016. Geochemical evidence of organic matter  
1052 source input and depositional environments in the lower and upper Eagle Ford Formation, south  
1053 Texas. *Organic Geochemistry* 98, 66–81.
- 1054 Takashima, R., Nishi, H., Huber, B., Leckie, R.M., 2006. Greenhouse World and the Mesozoic  
1055 Ocean. *Oceanography* 19, 82–92.
- 1056 Tappan, H., 1980. *Palaeobiology of Plant Protists*. W.H. Freeman & Co Ltd, San Francisco.
- 1057 Ten Haven, H.L., Deleeuw, J.W., Rullkotter, J., Damste, J.S.S., 1987. Restricted Utility of the  
1058 Pristane Phytane Ratio as a Palaeoenvironmental Indicator. *Nature* 330, 641–643.
- 1059 Ten Haven, H.L., Rohmer, M., Rullkotter, J., Bissert, P., 1989. Tetrahymanol, the Most Likely  
1060 Precursor of Gammacerane, Occurs Ubiquitously in Marine-Sediments. *Geochimica Et*  
1061 *Cosmochimica Acta* 53, 3073–3079.
- 1062 Tsikos, H., Jenkyns, H.C., Walsworth-Bell, B., Petrizzo, M.R., Forster, A., Kolonic, S., Erba, E., Silva,  
1063 I.P., Baas, M., Wagner, T., Damste, J.S.S., 2004. Carbon-isotope stratigraphy recorded by the  
1064 Cenomanian-Turonian Oceanic Anoxic Event: correlation and implications based on three key  
1065 localities. *Journal of the Geological Society* 161, 711–719.
- 1066 Turgeon, S.C., Creaser, R.A., 2008. Cretaceous oceanic anoxic event 2 triggered by a massive  
1067 magmatic episode. *Nature* 454, 323–326.
- 1068 Tyson, R., 1995. *Sedimentary Organic Matter: Organic facies and palynofacies*. Springer  
1069 Netherlands. doi:10.1007/978-94-011-0739-6
- 1070 Upchurch, G.R., Wolfe, J.A., 1993. Cretaceous Vegetation of the Western Interior and Adjacent  
1071 Regions of North America, in: *Evolution of the Western Interior Basin*, Geological Association of  
1072 Canada Special Paper. pp. 243–281.
- 1073 van de Schootbrugge, B., Bailey, T.R., Rosenthal, Y., Katz, M.E., Wright, J.D., Miller, K.G., Feist-  
1074 Burkhardt, S., Falkowski, P.G., 2005. Early Jurassic climate change and the radiation of organic-  
1075 walled phytoplankton in the Tethys Ocean. *Palaeobiology* 31, 73–97.

1076 van Helmond, N.A.G.M., Sluijs, A., Papadomanolaki, N.M., Plint, A.G., Grocke, D.R., Pearce, M.A.,  
 1077 Eldrett, J.S., Trabucho-Alexandre, J., Walaszczyk, I., van de Schootbrugge, B., Brinkhuis, H., 2016.  
 1078 Equatorward phytoplankton migration during a cold spell within the Late Cretaceous super-  
 1079 greenhouse. *Biogeosciences* 13, 2859–2872.

1080 van Helmond, N.A.G.M., Sluijs, A., Reichart, G.-J., Damsté, J.S.S., Slomp, C.P., Brinkhuis, H., 2014. A  
 1081 perturbed hydrological cycle during Oceanic Anoxic Event 2. *Geology* 42, 123–126.

1082 Varban, B.L., Plint, A.G., 2005. Allostratigraphy of the Kaskapau Formation (Cenomanian–  
 1083 Turonian) in the subsurface and outcrop: NE British Columbia and NW Alberta, Western Canada  
 1084 Foreland Basin. *Bulletin of Canadian Petroleum Geology* 53, 357–389.

1085 Varban, B.L., Plint, A.G., 2008a. Palaeoenvironments, palaeogeography, and physiography of a  
 1086 large, shallow, muddy ramp: Late Cenomanian-Turonian Kaskapau Formation, Western Canada  
 1087 foreland basin. *Sedimentology* 55, 201–233.

1088 Varban, B.L., Plint, A.G., 2008b. Sequence stacking patterns in the Western Canada foredeep:  
 1089 influence of tectonics, sediment loading and eustasy on deposition of the Upper Cretaceous  
 1090 Kaskapau and Cardium Formations. *Sedimentology* 55, 395–421.

1091 Vizcaíno, M., Yurchenko, I., Forkner, R., Fildani, A., Owens, J., Duncan, L., Sperling, E., 2020. Meta-  
 1092 Analysis Identifies Global and Regional Change during Cretaceous Ocean Anoxic Event 2.  
 1093 Presented at the Goldschmidt2020, p. 2689.

1094 Volkman, J., 2003. Sterols in microorganisms. *Applied Microbiology and Biotechnology* 60, 495–  
 1095 506.

1096 Volkman, J.K., Barrett, S.M., Dunstan, G.A., Jeffrey, S.W., 1994. Sterol biomarkers for microalgae  
 1097 from the green algal class Prasinophyceae. *Organic Geochemistry* 21, 1211–1218.

1098 Volkman, J.K., Barrett, S.M., Blackburn, S.I., Mansour, M.P., Sikes, E.L., and Gelin, F., 1998,  
 1099 Microalgal biomarkers: A review of recent research developments: *Organic Geochemistry*, v. 29,  
 1100 p. 1163–1179, doi:10.1016/S0146-  
 1101 6380(98)00062-X.

1102 Wells, M.L., Trainer, V.L., Smayda, T.J., Karlson, B.S.O., Trick, C.G., Kudela, R.M., Ishikawa, A.,  
 1103 Bernard, S., Wulff, A., Anderson, D.M., Cochlan, W.P., 2015. Harmful algal blooms and climate  
 1104 change: Learning from the past and present to forecast the future. *Harmful algae* 49, 68–93.

1105 West, O.L.O., Leckie, R.M., Schmidt, M., 1998. Foraminiferal Palaeoecology and  
 1106 Palaeoceanography of the Greenhorn Cycle Along the Southwestern Margin of the Western  
 1107 Interior Sea. doi:10.2110/csp.98.06.0079



- 1108 White, T., Arthur, M.A., 2006. Organic carbon production and preservation in response to sea-  
1109 level changes in the Turonian Carlile Formation, U.S. Western Interior Basin. *Palaeogeography,*  
1110 *Palaeoclimatology, Palaeoecology, Causes and Consequence of Marine Organic Carbon Burial*  
1111 *Through Time* 235, 223–244.
- 1112 White, T., Furlong, K., Arthur, M., 2002. Forebulge migration in the Cretaceous Western Interior  
1113 basin of the central United States. *Basin Research* 14, 43–54.
- 1114 Zeng, Z., Pike, M., Tice, M.M., Kelly, C., Marcantonio, F., Xu, G., Maulana, I., 2018. Iron fertilization  
1115 of primary productivity by volcanic ash in the Late Cretaceous (Cenomanian) Western Interior  
1116 Seaway. *Geology* 46, 859–862.
- 1117



## **1.9 Supplemental Material**

**Supplemental Materials:** Redox conditions and ecological resilience during Oceanic Anoxic Event 2 from the Western Interior Seaway

### **1.9.1 Supplemental material A: Sample Sites**

#### **1.9.1.1 Lohali Point**

The most southerly site, Lohali Point, is well-studied and described in terms of sedimentation and biostratigraphy (Elder, 1987; Kirkland, 1991, 1996; Leckie et al., 1991; Leckie et al., 1998). The section is located along the erosional scarp of eastern Black Mesa (36.183°N, 109.883°W), 6.5 km north-west of Lohali Point in north-eastern Arizona. The CTB is located within the Lower Mancos Shale, a 54.6 m thick unit comprising bioturbated, calcareous shales with numerous bentonites, calcisilts and concretion horizons (Leckie et al., 1991). These marker beds allow correlation to the time-equivalent lithostratigraphic units of the Bridge Creek Member, along with the uppermost few meters of the Hartland Shale Member and the basal few meters of the Fairport Member in central Colorado. A disconformity is noted at the CTB at Lohali Point, represented by a possible fine-grained sandstone gutter cast, 1 m across and 9 cm thick (Kirkland, 1996).

During the latest Cenomanian-middle Turonian Lohali Point is interpreted to be a neritic environment, at the distal end of a broad, shallow, seaward-sloping shelf that covered northern Arizona and south-central Utah (Grand Canyon Bight), and inwards of the forebulge trend (Kirkland, 1991; Leckie et al., 1991; Leithold, 1993; Leckie et al., 1998). It experienced relatively shallow water depths (<100 – 200 m: Sageman and Arthur, 1994), and relatively high sedimentation rates of 3.0 – 6.6 cm/kyr from fluvial input to the south (Leckie et al., 1998; Parker, 2016).

### 1.9.1.2 Gunnison Gorge

The Gunnison Gorge section is located just south of the Colorado State Highway 92 (38.7827°N, 107.86898°W), 17 km east of Delta, Colorado. At this location the Bridge Creek Member is a fissile, grey, moderately calcareous, silty shale containing approximately 10–12 zones of orange-grey concretions of up to 1 m diameter. Numerous bentonites and limestone beds occur towards the top of the section, including a prominent 10 cm continuous limestone bench (Figure 3C.1) and a 2 m long, 3 cm thick lens of jet. Fossils of oysters (*Pycnodonte* aff. *P. newberryi*) are found within the top of the Bridge Creek Member, but are more commonly found in the overlying Fairport Member.

The Gunnison Gorge section represents a relatively proximal site that was located on a large palaeo-bathymetric high of <50 m water depths (often described as site of lacuna). This high was created by the rising basin forebulge (White et al., 2002) and was found across eastern Utah, north-western Colorado and southwestern Wyoming (Merewether and Cobban, 1986; Elder and Kirkland, 1993; Sageman and Arthur, 1994; Slingerland et al., 1996; Arthur and Sageman, 2005).

#### Gunnison Gorge



**Figure 3C.1:** Approximately 8 cm thick limestone bed with an erosive base and mud rip-up clasts. The base of this bed represents a disconformity, resulting in the absence of sediments deposited during OAE2.

#### **1.9.1.3 Rebecca Bounds**

The Rebecca Bounds core is located in westernmost Kansas (38.489628°N, 101.974552°W). Samples were acquired from the Lincoln, Hartland and Bridge Creek members of the Greenhorn Formation at the USGS Core Repository Centre in Denver. The Lincoln Limestone is a 7.9 m dark-grey calcareous shale underlying the 5.2 m darker-grey calcareous shale of the Hartland Shale. The overlying Bridge Creek Member consists of 25 m of decimetre-meter scale interbedded limestone-shale, or chalk-marl, couplets, with the shale and marl units grading up into limestone beds. Contacts between limestone beds and the overlying shales are generally sharp, however some are burrowed and appear gradational (Scott, 1998).

The Rebecca Bounds core was located in the distal axial basin (White and Arthur, 2006), and experienced greater water depths (<200 – 300 m) (Sageman and Arthur, 1994) than the other sites in this study.

#### **1.9.1.4 Billings Landfill**

Samples from the western side of Billings Landfill, Montana (45.72°N, 108.56°W) preserve the Belle Fourche Formation and Lower Shale Member of the Greenhorn Formation. Dark non-calcareous shale of the Belle Fourche Formation is found at the base and includes sparse molluscan fossils and a fossiliferous lag associated with gutter casts. Overlying this, the tan-weathering Lower Shale Member of the Greenhorn Formation comprises calcareous silty shale with occasional bentonites (Flogel, 2001).

The Billings Landfill site was at a proximal location inwards of the basin forebulge, with relatively shallow water depths of <100 m (Sageman and Arthur, 1994). At different times it shared

foraminiferal traits with either the northern Boreal or the southern Tethyan WIS, suggesting that a mixing front between the two water masses influenced this site (Dameron et al., in press). The occurrence of ripples, silt laminae and gutter casts throughout the section support the presence of strong bottom water currents, which may be related to incursions of Tethyan waters (Dameron et al., in press).

#### **1.9.1.5      Pratts Landing**

The most northern site, Pratts Landing, is located on the north bank of the Peace River (56.020556°N, 118.813056°W) in north-western Alberta (van Helmond et al., 2016). It comprises stacked silty and sandy upward-coarsening successions of the Sunkay Member, capped at a prominent flooding surface by weakly bioturbated, organic-rich claystones and silty claystones of the Vimy Member. An unconformity inferred from inoceramid biostratigraphy has been identified within the lower part of the Vimy Member at the CTB (van Helmond et al., 2016).

Pratts Landing was located close to the forebulge, on the eastern flank of the foredeep, approximately 160 km from the WIS shoreline (Varban and Plint, 2005, 2008b). Here, shallow water depths (<70 m) allowed storm-wave and current reworking of sediments (Plint et al., 2012). Wireline log data has allowed strata to be correlated across the foredeep to the east, and identified a minor hiatus in the earliest Turonian (van Helmond et al., 2016).

### **1.9.2      Supplemental material B: Further proxy information**

#### **1.9.2.1      Terrestrial input**

**TAR:** Higher plants produce *n*-alkanes with a strong predominance of odd over even numbered carbon chain lengths.  $nC_{27}$ ,  $nC_{29}$ , and  $nC_{31}$  in particular are attributed to epicuticular waxes from vascular plant organic material, with lower molecular weight *n*-alkanes (e.g.  $nC_{17}$ ) more indicative of aquatic organic matter (Bourbonniere and Meyers, 1996; Peters et al., 2005). A number of comparison ratios have been established to measure the differing distributions of *n*-alkanes and

establish the dominance of terrestrial vs marine organic matter (e.g. carbon preference index, odd-over-even predominance, terrigenous/aquatic ratio): (Bray and Evans, 1961; Scalan and Smith, 1970; Herrera-Herrera et al., 2020). For this study the terrigenous/aquatic ratio has been used as it specifically compares the vascular plant *n*-alkanes with more marine indicative lower weight *n*-alkanes.

**Oleanane Index:** Oleanane is formed within specific angiosperms (flowering land plants) and its presence therefore indicative of terrestrial organic matter input, often within deltaic settings (Riva et al., 1988; Ekweozor and Telnaes, 1990; Moldowan et al., 1994; Peters et al., 2005). Whilst it has been identified in older sediments, angiosperms did not become prominent until the Late Cretaceous so may also be used as an age-marker.

**T:M:** the ratio of terrigenous (phytoclads, pollen, spores) to marine (dinoflagellates, prasinophytes, acritarchs) palynomorphs can be used to assess the relative distributions of organic matter from the continental and marine environments.

#### **1.9.2.2 Redox**

**Pr/ph:** Pristane (pr) and phytane (ph) are predominantly derived from the phytol side chain of chlorophylls a and b, and bacteriochlorophylls a and b from a range of bacteria (Brooks et al., 1969; Powell and McKirdy, 1973), and their use as a redox proxy stems from the differing breakdown pathways of its derivative phytol molecule. Under anoxic conditions phytol is reduced and dehydrated to become phytane, however under oxic conditions phytol undergoes a pathway of oxidation, decarboxylation and reduction to become pristane. Didyk et al. (1978) therefore proposed this ratio to assess redox conditions at the sediment-water interface, with values of <1 indicating anoxia, and higher values suggestive of oxidising conditions. Care should be used when using the pr/ph ratio as both molecules can derive from sources other than phytol, such as phytane from archaea (Ten Haven et al., 1987) or pristane from zooplankton, or tocopherols from most photosynthesizing organisms (Goossens et al., 1984).

**C<sub>34</sub>/C<sub>35</sub> HH:** C<sub>31</sub>-C<sub>35</sub> homohopanes derive from bacteriohopanepolyols produced by many bacteria (Peters et al., 2005). Higher molecular weight C<sub>35</sub> homohopanes are preferentially preserved under reducing conditions, and so the ratio of C<sub>35</sub> to other homohopanes can be an indicator of depositional redox conditions. The homohopane index is generally measured as C<sub>35</sub>/(C<sub>31</sub>-C<sub>35</sub>) homohopanes, or C<sub>35</sub>/C<sub>34</sub> homohopane. In this study we have used C<sub>34</sub>/C<sub>35</sub> homohopane so that redox trends match those of pr/ph (i.e. lower values indicate more anoxic conditions). This proxy is affected by thermal maturity, and generally C<sub>35</sub> homohopanes are more predominant in carbonate lithologies compared to shales.

**Isorenieratane:** Isorenieratane is a carotenoid derived from brown-pigmented green sulphur bacteria (*Chlorobiaceae*), an obligate anaerobic photoautotrophic organism that requires both light and hydrogen sulphide (Summons and Powell, 1987; Sinninghe Damsté et al., 1993; Grice et al., 1996). Therefore the presence of this molecule is indicative of Photic Zone Euxinia (PZE) a phenomenon where euxinic waters reach the photic zone of a water column (Sinninghe Damsté and Schouten, 2006; Meyer and Kump, 2008). Isorenieratane can, however, derive from other sources, and compound specific isotope analysis is necessary to have full confidence of a *Chlorobiaceae* source (Koopmans et al., 1996).

#### 1.9.2.3 Stratification

**Gammacerane:** Gammacerane is formed from tetrahymol, a molecule that is biosynthesised by bacterivorous marine ciliates in the absence of steroid-rich algae at the interface between oxic and anoxic zones in stratified water columns (Li, 1989; Ten Haven et al., 1989; Damsté et al., 1995). Gammacerane can occur in many sediments, albeit in trace amounts (Ten Haven et al., 1989). It occurs in high amounts in hypersaline environments and was thus initially used as a palaeosalinity proxy (Sinninghe Damsté et al., 1995), although now considered a useful proxy more generally for stratified water columns (Peters et al., 2005). However, it is important to recognize that tetrahymanol has also been found in anaerobic fungus, freshwater ciliates, photosynthetic bacteria, a fern species, and in marine ciliates when their diet is deprived of sterols and they consume prokaryotes (Peters et al., 2005 and refs therein).



#### 1.9.2.4 Ecological change

**St/H:** Steranes (St) largely derive from eukaryotic organisms (predominantly algae and higher plants), whereas hopanes (H) mostly derive from bacteria (Peters et al., 2005). Therefore, the St/H ratio can be used to assess the relative contribution of these sources. For this study, the ratio of all regular  $\alpha\alpha\alpha$  steranes, over all regular hopanes has been used.

**Sterane abundance:** Eukaryotes use steroids within their cell walls, and derivatives of these steroids, steranes, are ubiquitous in marine and lacustrine sedimentary records (Volkman, 2003; Peters et al., 2005).  $C_{27}$ ,  $C_{28}$  and  $C_{29}$  steranes are derived predominantly from red algae, chlorophyll c-containing algae (such as prasinophytes) and green algae/terrestrial plants, respectively (W. Y. Huang and Meinschein, 1979; Tissot and Welte, 1984; Volkman, 1986; Schwark and Emt, 2006; Knoll et al., 2007; Kodner et al., 2008). See Discussion in Main Text for more information.

**Prasinophyte (%):** Prasinophytes are simple unicellular green algae, that are often present in abundance under harsh environmental conditions that other organisms could not tolerate. See Discussion in Main Text for more information.

### **1.9.3 Supplemental material C: Methods**

#### **1.9.3.1 Bulk TOC, $\delta^{13}\text{C}$ and elemental geochemistry**

The outer rims of rock samples were trimmed with a saw, and the interiors powdered using a benchtop IKA-WERKE grinder. Calcium carbonate ( $\text{CaCO}_3$ ) was removed by reacting the powdered sample with 40% HCl for 24 hours, and then diluting and centrifuging with de-ionised water until a neutral pH was attained. An Isoprime vision Isotope Ratio Mass Spectrometer coupled with an Elementar PYRO Cube Elemental Analyser (EA-IRMS) was then used to measure total residue carbon ( $\text{TC}_{\text{res}}$ ) and the carbon isotopic composition of bulk organic matter ( $\delta^{13}\text{C}_{\text{org}}$ ). The elemental standard acetanilide was used for  $\text{TC}_{\text{res}}$  and  $\delta^{13}\text{C}_{\text{org}}$  data were calibrated with international reference materials USGS-40 and USGS-41a, with precision of 0.61 % for TC and average 0.25 ‰ for  $\delta^{13}\text{C}_{\text{org}}$ .  $\text{CaCO}_3$  content was calculated using the change in dry weight following decarbonation, and cross checked against a subset of samples where the total inorganic carbon (TIC) was measured in duplicate using a UIC CM5015  $\text{CO}_2$  Coulometer. Total organic carbon (TOC) was calculated based upon the dry-weight difference of TC and TIC.

#### **1.9.3.2 Lipid biomarkers**

Organic matter from 5–15g of powdered rock was extracted using a Thermo 250 Accelerated Solvent Extractor with a dichloromethane:methanol (DCM:MeOH) ratio of 9:1 (v/v). The total lipid extract was then dried to organic residues using a Genevac EZ-2 vacuum centrifuge. The aliphatic, aromatic and polar fractions were eluted with hexane, hexane:DCM (4:1, v/v) and DCM:MeOH (1:1, v/v) respectively using silica column separation with 3 dead volumes.

A Thermo Trace 1310 Gas Chromatograph coupled to a Thermo TSQ8000 Mass Spectrometer (GC-MS) at the University of Southampton was used to analyse the aliphatic and aromatic fractions, with helium used as a carrier gas at a flow rate of 1.2ml/min. The column was a DB-5 (30 m; 0.25 mm i.d.; 0.25  $\mu\text{m}$  film thickness). The GC oven temperature program consisted of heating to 40°C for 2 minutes, a temperature ramp to 310°C at a rate of 6°C/min, and holding for 15 minutes, with a total program lasting 62 minutes. The Norwegian Geochemical Standard North Sea Oil was analysed within each run of the GC-MS and used as a standard to identify peak retention times.

The aliphatic fractions were run at full-scan and Selected Ion Monitoring of 57 (*n*-alkanes), 191 (hopanes) and 217 (steranes), as well as GCMS-MS on 412 to 191 to elucidate co-eluting hopane peaks. The aromatic fractions were run at full scan and Selected Ion Monitoring of 133/134 (isorenieratane), and compared against an in-house standard with known retention times for isorenieratane and its derivatives. The isorenieratane molecule itself was not clear in any samples, however, derivative molecules were found. Isorenieratane was classified as present if there was a clear peak at the known retention time for isorenieratane derivatives with 133/134 ions dominant in the mass spectra, trace if a smaller peak was present with 133/134 ions present, and absent if no peak was seen at the known retention time for isorenieratane derivatives (see Supplemental Material D: Identifying isorenieratane). Raney-Nickel analysis from previous studies indicate that no isorenieratane is contained within the sulphur-bound organic matter (Simons and Kenig, 2001), and therefore no Raney-Nickel analyses were performed as part of this study.

### **1.9.3.3 Palynology**

For the Lohali Point, Gunnison Gorge, Rebecca Bounds and Billings sites, between 2–5g of rock material was broken into fragments <1cm<sup>3</sup>. These were dosed in 30% hydrochloric acid for 24 hours and washed until pH-neutral to remove carbonates. This procedure was repeated using 60% hydrofluoric acid to remove silicates. The sample was then sieved through a nylon mesh to retain the >15 µm fraction which was then briefly boiled in 30% HCl to solubilise neo-formed fluorides before rapid dilution and further sieving. A tunable ultrasonic probe was used for up to 45 seconds to disaggregate the amorphous organic matter (AOM) as necessary. Samples were mounted on glass coverslips after a final sieving, left to dry, and then inverted onto glass microscope slides with Elvacite 2044 as the mountant. At least 150 particles were counted per sample to generate palynofacies data, and the continental/marine (C/M) ratio calculated as (phytoclasts + pollen + spores) / (phytoclasts + pollen + spores + dinocysts + acritarchs + others). Palynofacies data for Pratts Landing were generated using the methods detailed in van Helmond et al. (2016), where the C/M ratio was calculated as (pollen + spores) / (pollen + spores + dinocysts + acritarchs + others). Prasinophyte data were not collected for Pratts Landing.

#### **1.9.3.4 Nannofossils**

Calcareous nannofossil biostratigraphy was generated using smear slides and standard light microscope techniques (Bown and Young 1998). A sediment-water slurry was smeared over a cover slide, rapidly dried, and glued to a glass slide using Norland Optical Adhesive, fixed under UV light. Stratigraphic distribution data was collected semi-quantitatively using a Zeiss Axiophot photomicroscope at x1,000 magnification. Species abundances were estimated per field of view (FOV) after looking at around five slide transects (equating to thousands of fields of view).

Taxonomy generally follows Bown (1998) and Nannotax (<http://www.mikrotax.org/Nannotax3>).

The relative abundance of each species was recorded as follows: R = Rare (<1 per 10 FOV – fields of view), F = Few (1 per 10 FOV), C = Common (1-9 per FOV), A = Abundant (>10 per FOV).

Nannofossil biostratigraphy is described with reference to the Upper Cretaceous zones of Burnett (1998).

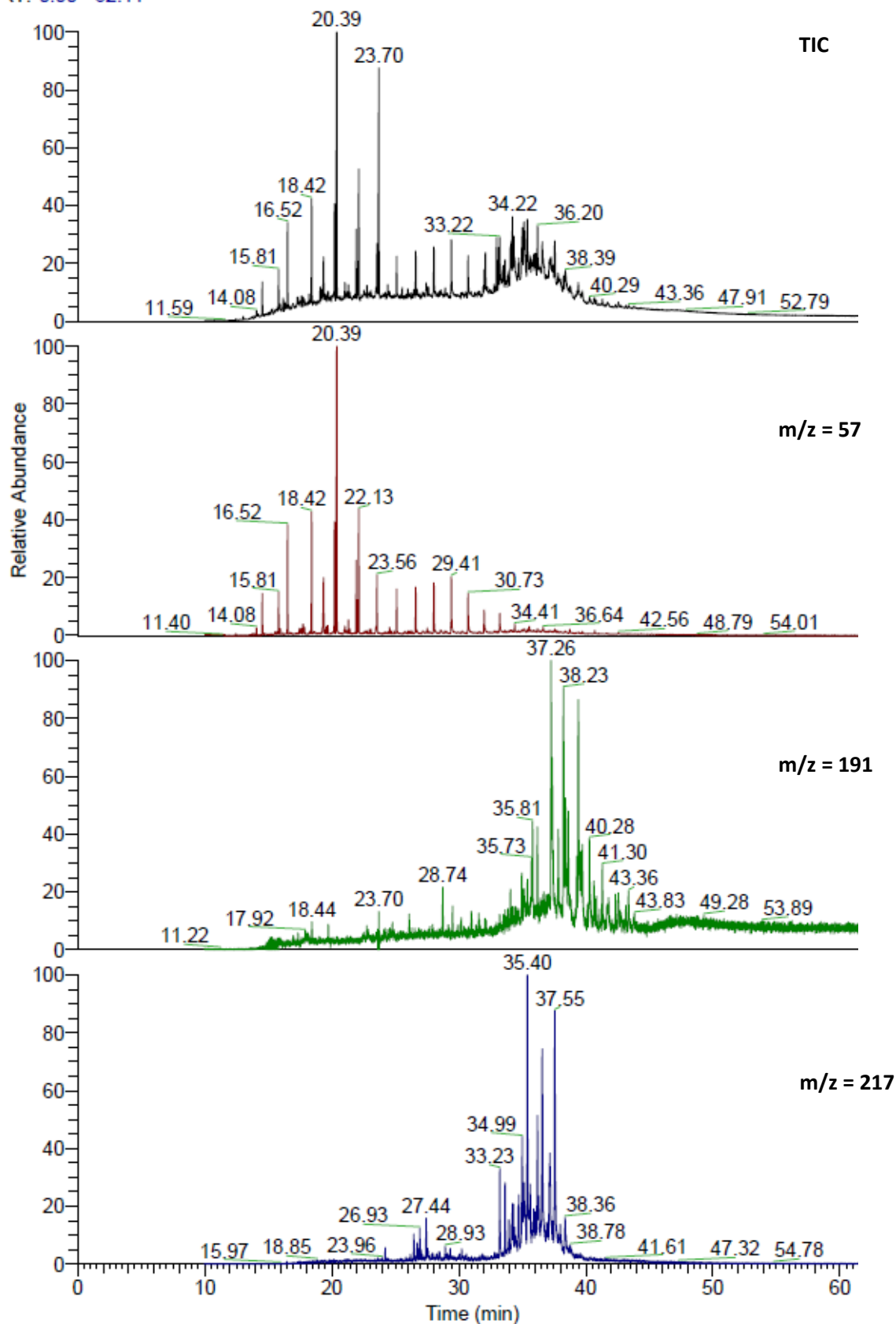
#### **1.9.3.5 Principle Component Analysis (PCA)**

Principle Component Analysis (PCA) was undertaken at each of the five sites using lipid biomarker and palynological data. The lipid biomarker variables comprised selected proxies for redox (Pr/Ph and  $C_{34}/C_{35}$  HH), stratification (Gammacerane Index), terrestrial organic matter (Oleanane Index, TAR) and eukaryotic abundance ( $C_{27}$ – $C_{29}$  steranes). The palynological variables comprised proxies for terrestrial organic matter (C/M) and prasinophyte abundance. The Pratts Landing dataset did not contain prasinophyte data, and therefore this proxy is absent from the Pratts Landing PCA results.

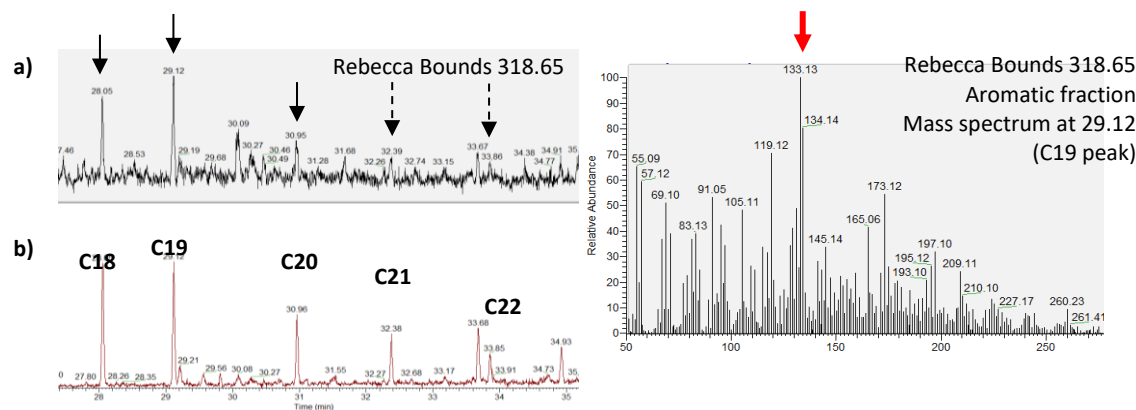
### 1.9.5 Supplemental material D: Typical chromatogram

Typical aliphatic total ion chromatogram and mass chromatograms used to identify alkanes ( $m/z$  57), hopanes ( $m/z$  191) and steranes (217), from Rebecca Bounds sample at 299.9 m depth.

RT: 0.00 - 62.11

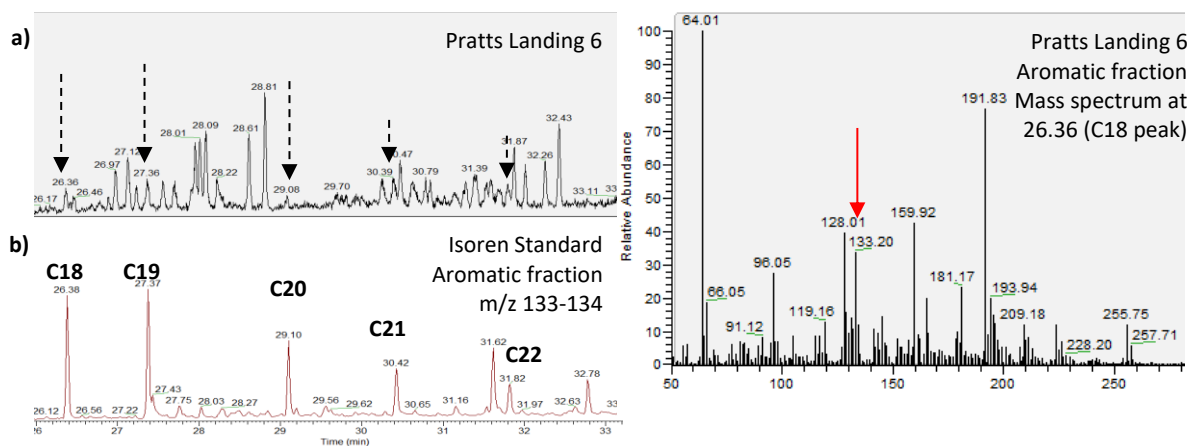


### 1.9.6 Supplemental Material E: Identifying isorenieratane



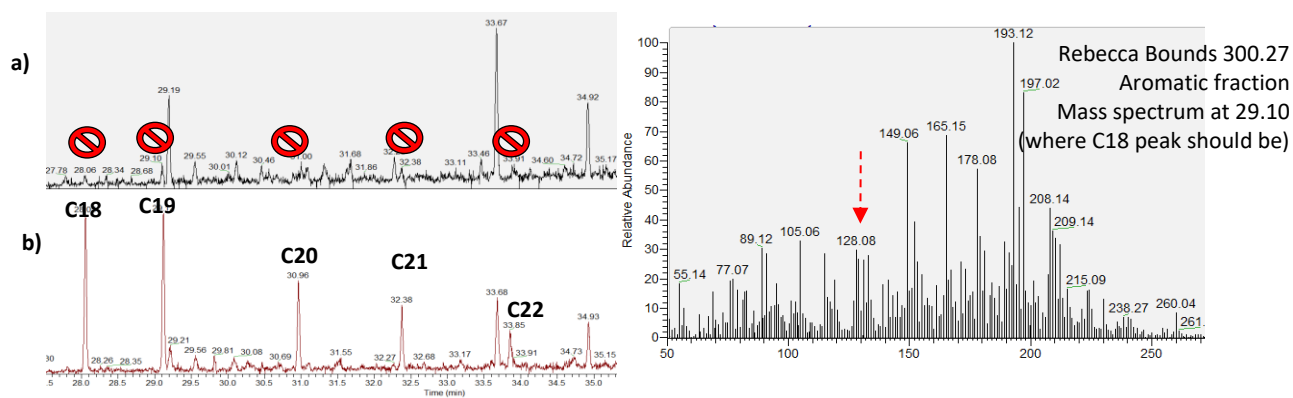
**Isorenieratane = Present:** Mass chromatogram ( $m/z$  133/134) of a) Rebecca Bounds 318.65, and b) isorenieratane standard. Clear peaks are identified at the same retention times as isorenieratane diagenetic products (aryl and diaryl isoprenoids).

**Isorenieratane = Present:** 133 and 134 are dominant fragment ions within the mass spectrum.



**Isorenieratane = Trace:** Mass chromatogram ( $m/z$  133/134) of a) Pratts Landing 6, and b) isorenieratane standard. Peaks are identified at the same retention times as isorenieratane diagenetic products (aryl and diaryl isoprenoids).

**Isorenieratane = Trace:** 133 and 134 form minor peaks in the fragment ions of the mass spectrum.

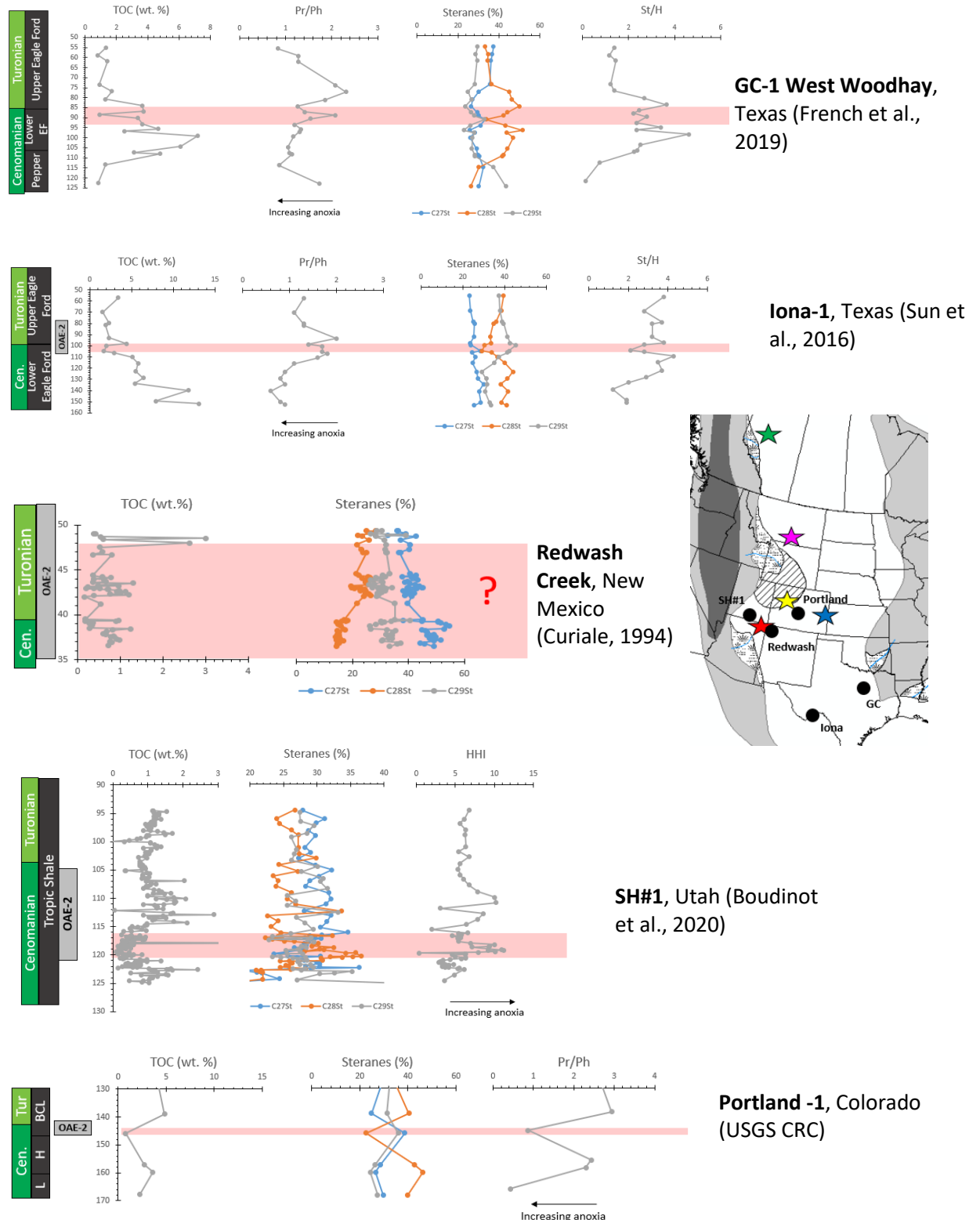


**Isorenieratane = Absent:** Mass chromatogram (m/z 133/134) of a) Rebecca Bounds 300.27, and b) isorenieratane standard. No clear peaks are identified at the same retention times as isorenieratane diagenetic products (aryl and diaryl isoprenoids).

**Isorenieratane = Absent:** 133 and 134 ions not clearly present, and part of spectrum 'noise'

## 1.9.7 Supplemental Material F: Cenomanian-Turonian data for five published sites

Data for five CTB sites in the WIS, showing TOC, relative sterane abundance and redox proxy, where available. Where identified, the position of OAE2 is marked on the section and red box indicates hypothesized Benthonic Zone, based upon low, or decreasing, C<sub>28</sub> sterane abundance and low TOC. Additionally, the Benthonic Zone is identified through foraminiferal analysis in the SH#1 core in Utah.



### 1.9.8 Supplementary Material G: References

#### References for Supplementary Materials

- Boudinot, F.G., Dildar, N., Leckie, R.M., Parker, A., Jones, M.M., Sageman, B.B., Bralower, T.J., Sepúlveda, J., 2020. Neritic ecosystem response to Oceanic Anoxic Event 2 in the Cretaceous Western Interior Seaway, USA. *Palaeogeography, Palaeoclimatology, Palaeoecology* 546, 109673.
- Bourbonniere, R.A., Meyers, P.A., 1996. Anthropogenic influences on hydrocarbon contents of sediments deposited in eastern Lake Ontario since 1800. *Environmental Geology* 28, 22–28.
- Bray, E.E., Evans, E.D., 1961. Distribution of n-paraffins as a clue to recognition of source beds. *Geochimica et Cosmochimica Acta* 22, 2–15.
- Brooks, J.D., Gould, K., Smith, J.W., 1969. Isoprenoid Hydrocarbons in Coal and Petroleum. *Nature* 222, 257–259.
- Curiale, J.A., 1994. Geochemical Anomalies at the Cenomanian-Turonian Boundary, Northwest New-Mexico. *Organic Geochemistry* 22, 487–500.
- Damste, J.S.S., Kenig, F., Koopmans, M.P., Koster, J., Schouten, S., Hayes, J.M., Deleeuw, J.W., 1995. Evidence for Gammacerane as an Indicator of Water Column Stratification. *Geochimica Et Cosmochimica Acta* 59, 1895–1900.
- Ekweozor, C.M., Telnaes, N., 1990. Oleanane Parameter - Verification by Quantitative Study of the Biomarker Occurrence in Sediments of the Niger Delta. *Organic Geochemistry* 16, 401–413.
- French, K.L., Birdwell, J.E., Whidden, K.J., 2019. Geochemistry of a thermally immature Eagle Ford Group drill core in central Texas. *Organic Geochemistry* 131, 19–33.
- Goossens, H., de Leeuw, J.W., Schenck, P.A., Brassell, S.C., 1984. Tocopherols as likely precursors of pristane in ancient sediments and crude oils. *Nature* 312, 440–442.
- Herrera-Herrera, A.V., Leierer, L., Jambriña-Enríquez, M., Connolly, R., Mallol, C., 2020. Evaluating different methods for calculating the Carbon Preference Index (CPI): Implications for palaeoecological and archaeological research. *Organic Geochemistry* 146, 104056.
- Huang, W.Y., Meinschein, W.G., 1979. Sterols as Ecological Indicators. *Geochimica Et Cosmochimica Acta* 43, 739–745.
- Knoll, A.H., Summons, R.E., Waldbauer, J.R., Zumberge, J.E., 2007. CHAPTER 8 - The Geological Succession of Primary Producers in the Oceans, in: Falkowski, P.G., Knoll, Andrew H. (Eds.), *Evolution of Primary Producers in the Sea*. Academic Press, Burlington, pp. 133–163.



- Kodner, R.B., Pearson, A., Summons, R.E., Knoll, A.H., 2008. Sterols in red and green algae: quantification, phylogeny, and relevance for the interpretation of geologic steranes. *Geobiology* 6, 411–420.
- Koopmans, Martin P., Köster, J., Van Kaam-Peters, H.M.E., Kenig, F., Schouten, S., Hartgers, W.A., de Leeuw, J.W., Sinninghe Damsté, J.S., 1996. Diagenetic and catagenetic products of isorenieratene: Molecular indicators for photic zone anoxia. *Geochimica et Cosmochimica Acta* 60, 4467–4496.
- Koopmans, M. P., Schouten, S., Kohnen, M.E.L., Damste, J.S.S., 1996. Restricted utility of aryl isoprenoids as indicators for photic zone anoxia. *Geochimica Et Cosmochimica Acta* 60, 4873–4876.
- Li, R.W., 1989. Geological Occurrence and Its Palaeoenvironmental Significance of Gammacerane. *Chinese Science Bulletin* 34, 1208–1211.
- Meyer, K.M., Kump, L.R., 2008. Oceanic Euxinia in Earth History: Causes and Consequences. *Annual Review of Earth and Planetary Sciences* 36, 251–288.
- Moldowan, J.M., Dahl, J., Huizinga, B.J., Fago, F.J., Hickey, L.J., Peakman, T.M., Taylor, D.W., 1994. The Molecular Fossil Record of Oleanane and Its Relation to Angiosperms. *Science* 265, 768–771.
- Peters, C.C., Walters, C., Moldowan, J.M., 2005. *The Biomarker Guide: Volume II. Biomarkers and Isotopes in Petroleum Systems and Earth History*. Cambridge University Press.
- Powell, T.G., McKirdy, D.M., 1973. Relationship between Ratio of Pristane to Phytane, Crude Oil Composition and Geological Environment in Australia. *Nature Physical Science* 243, 37–39.
- Riva, A., Caccialanza, P.G., Quagliaroli, F., 1988. Recognition of 18 $\beta$  (H)oleanane in several crudes and Tertiary-Upper Cretaceous sediments. Definition of a new maturity parameter. *Organic Geochemistry, Proceedings of the 13th International Meeting on Organic Geochemistry* 13, 671–675.
- Scalan, E.S., Smith, J.E., 1970. An improved measure of the odd-even predominance in the normal alkanes of sediment extracts and petroleum. *Geochimica et Cosmochimica Acta* 34, 611–620.
- Schwark, L., Empt, P., 2006. Sterane biomarkers as indicators of palaeozoic algal evolution and extinction events. *Palaeogeography, Palaeoclimatology, Palaeoecology, Evolution of the System Earth in the Late Palaeozoic: Clues from Sedimentary Geochemistry* 240, 225–236.

Sinninghe Damsté, J.S., Kenig, F., Koopmans, M.P., Köster, J., Schouten, S., Hayes, J.M., de Leeuw, J.W., 1995. Evidence for gammacerane as an indicator of water column stratification. *Geochimica et Cosmochimica Acta* 59, 1895–1900.

Sinninghe Damsté, J.S., Schouten, S., 2006. Biological Markers for Anoxia in the Photic Zone of the Water Column, in: Volkman, J.K. (Ed.), *Marine Organic Matter: Biomarkers, Isotopes and DNA*, The Handbook of Environmental Chemistry. Springer, Berlin, Heidelberg, pp. 127–163.

Sinninghe Damsté, J.S., Wakeham, S.G., Kohnen, M.E.L., Hayes, J.M., de Leeuw, J.W., 1993. A 6,000–year sedimentary molecular record of chemocline excursions in the Black Sea. *Nature* 362, 827–829.

Summons, R.E., Powell, T.G., 1987. Identification of Aryl Isoprenoids in Source Rocks and Crude Oils - Biological Markers for the Green Sulfur Bacteria. *Geochimica Et Cosmochimica Acta* 51, 557–566.

Sun, X., Zhang, T., Sun, Y., Milliken, K.L., Sun, D., 2016. Geochemical evidence of organic matter source input and depositional environments in the lower and upper Eagle Ford Formation, south Texas. *Organic Geochemistry* 98, 66–81.

Ten Haven, H.L., Deleeuw, J.W., Rullkotter, J., Damste, J.S.S., 1987. Restricted Utility of the Pristane Phytane Ratio as a Palaeoenvironmental Indicator. *Nature* 330, 641–643.

Ten Haven, H.L., Rohmer, M., Rullkotter, J., Bissere, P., 1989. Tetrahymanol, the Most Likely Precursor of Gammacerane, Occurs Ubiquitously in Marine-Sediments. *Geochimica Et Cosmochimica Acta* 53, 3073–3079.

Tissot, B.P., Welte, D.H., 1984. Production and Accumulation of Organic Matter The Organic Carbon Cycle, in: Tissot, B.P., Welte, D.H. (Eds.), *Petroleum Formation and Occurrence*. Springer, Berlin, Heidelberg, pp. 3–13.

USGS Core Research Centre Data repository [WWW Document], n.d. URL <https://my.usgs.gov/crcwc/>

Volkman, J., 2003. Sterols in microorganisms. *Applied Microbiology and Biotechnology* 60, 495–506.

Volkman, J.K., 1986. A Review of Sterol Markers for Marine and Terrigenous Organic-Matter. *Organic Geochemistry* 9, 83–99.